Journal of Hydrology 641 (2024) 131806

Contents lists available at ScienceDirect

Journal of Hydrology

journal homepage: www.elsevier.com/locate/jhydrol

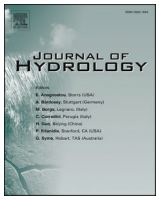

Research papers

Tiny rain makers: How aerosols shape extreme rainfall simulation accuracy

Ying Liu [a,*], Hai Liu [a], Lu Zhuo [a,b], Dawei Han [a]

[a] School of Civil, Aerospace and Mechanical Engineering, University of Bristol, Bristol, BS8 1TR
[b] School of Earth and Environmental Sciences, Cardiff University, Cardiff CF10 3AT, UK

ARTICLE INFO

This manuscript was handled by Andras Bardossy, Editor-in-Chief, with the assistance of Gerald Augusto Corzo, Associate Editor

Keywords:
Rainfall simulation
Aerosol properties
Aerosol transport
Seasonality
WRF-Chem

ABSTRACT

Given the rapid spatiotemporal variability of aerosols and their complex impacts on the Earth system, investigating the role of aerosols in modelling extreme weather events, particularly various extreme rainfalls, remains limited. This study explored extreme rainfall simulation sensitivity to aerosol properties, transport and seasonality over the UK and Ireland during four seasons in 2020 by the Weather Research and Forecasting model coupled with Chemistry (WRF-Chem) model. Two sets of high-resolution simulations, one including aerosol direct and indirect effects and the other one without any aerosol effects, were conducted to investigate the improvements due to aerosol inputs. Meteorological results were verified using ground and satellite observations to examine the reliability of simulations. The 12 extreme rainfall events during the study months were classified by their backward trajectories from the Hybrid Single-Particle Lagrangian Integrated Trajectory (HYSPLIT) model, and their simulation accuracies were quantified through six spatiotemporal metrics and one overall score. By comprehensive analyses of the simulation performances under different conditions, it is found that the model performs better in simulating rainfall events driven by sea salt aerosols (SSA) compared to those promoted by anthropogenic aerosols. Air masses transported from the Arctic and North Atlantic Ocean also help achieve higher rainfall simulation accuracy than European air masses. Rainfall simulations for winter and autumn events outperform those for spring and summer events. When considering aerosol effects in simulations, almost half of the events showed improved performance, while an equal number experienced a decrease and a small proportion remained unchanged. The most remarkable improvements are observed in rainfall simulations with higher concentrations of SSA and the participation of anthropogenic aerosols, while simulations promoted only by anthropogenic aerosols all experience performance reductions. The aerosol effects also led to significant increases in monthly rainfalls, accompanied by great reductions of Cl in larger particle size aerosols and NO_3 in smaller particle size aerosols.

1. Introduction

Atmospheric aerosols, the liquid or solid particulate matter in the atmosphere, play an important role in the weather and climate at regional and global scales. The influence of atmospheric aerosols on precipitation patterns, especially on extreme rainfall events, is a critical area of study within atmospheric science. Aerosols affect not only the microphysical properties of clouds but also have broader implications for storms' scale and intensity. The direct effect of aerosols through scattering and absorbing solar radiations leads to decreases in wind speed, surface temperature and the height of the planetary boundary layer (PBL) while increasing relative humidity (RH) and atmospheric stability (Jacobson et al., 2007). The indirect effect of aerosols through serving as cloud condensation nuclei (CCN) results in a reduction in cloud droplet size and a rise in cloud droplet number concentration (CDNC), precipitation, cloud coverage and lifetime of low-level clouds (Albrecht, 1989). The aerosol-cloud-precipitation-meteorology interaction and feedback have been observed in many field experiments by various satellites and surface networks (Ramanathan and Carmichael, 2008; Rosenfeld et al., 2007, 2008; Zanis, 2009; Levin and Brenguier, 2009).

The assessment of aerosol impacts is challenging because these particles not only have large spatiotemporal variability and short lifetimes, but also have sizes that span several orders of magnitude and complex physical and chemical properties. The fine-mode particles with a diameter less or equal to 2.5 μm (PM2.5) are composed of various chemical compounds such as nitrate (NO_3), ammonium (NH_4), sulfate (SO_4) and organic and black carbon (OC and BC). Sea salt aerosols

* Corresponding author.
E-mail address: emily.liu@bristol.ac.uk (Y. Liu).

https://doi.org/10.1016/j.jhydrol.2024.131806
Received 18 March 2024; Accepted 29 July 2024
Available online 11 August 2024

(primarily composed of Na^+ and Cl^-) and some species from soil dust are usually in coarse mode. Apart from primary aerosols (e.g., BC, OC, sea salt and dust) that are emitted directly into the atmosphere, a large part of the aerosol mass is secondary aerosols (e.g. NO_3, NH_4, SO_4 and secondary organic aerosol (SOA)) that are formed by chemical reactions from its gaseous precursors such as NOx, NH3 and SO2. As noted by Lohmann and Feichter (2005) and Chen et al. (2008), the magnitude of the aerosol semi-direct and indirect effects is influenced by the particle size, number concentration and composition of the atmospheric aerosols that serve as CCN or ice nuclei (IN). Particles containing hygroscopic components like water-soluble ions (e.g., Na^+, Cl^-, NO_3^-, SO_4^{2-}) readily act as CCN (Chen and Lamb, 1994). On the contrary, hydrophobic components such as elemental carbon must be wrapped by hygroscopic substances before they become CCN (Dusek et al., 2006). Furthermore, the transformation of primary aerosols into secondary aerosols also changes aerosol properties, which greatly impacts cloud-aerosol interactions and subsequent rainfall patterns. For example, SSA can react with various atmospheric compounds and form new aerosol types like sodium nitrate ($NaNO_3$), sodium sulfate (Na_2SO_4) and internal mixtures. This transformation process is known as the "ageing of sea spray aerosol". Hung et al. (2016) noted an increasing trend of $NaNO_3$ absorbance at particle diameter ≥ 1 μm due to the reaction of nitric acid with SSA. In addition, Zieger et al. (2017) demonstrate that the hygroscopic growth of inorganic sea salt is lower than pure sea salt particles. They also observed an increase in hygroscopic growth with decreasing particle size (for particle diameters < 0.15 μm) and this increase is independent of the particle generation method. According to previous studies, the hygroscopicity and optical properties of aged SSA depend on the changes in chemical composition, mixing state and particle size of SSA before and after ageing (Carrico et al., 2003; Randles et al., 2004; Bougiatioti et al., 2011; Schill et al., 2015; Rosati et al., 2021). Therefore, the aged aerosols often have distinctly different properties and will lead to unpredictable impacts on cloud droplets, cloud albedo and amount of rainfall.

In addition to understanding aerosol properties, aerosol transport is critical to determining the impact of atmospheric emissions and improving meteorological models. Pollutants, bacteria and nutrients can be transported through the atmosphere over large distances across the globe (e.g., Lindqvist et al., 1991; Artaxo et al., 1994; Maki et al., 2019). Braun et al. (2020) evaluated the influences of local and long-range transport of aerosol to the Philippines during monsoon seasons under various synoptic- and local-scale conditions. They found that the events affected by biomass burning transport had the highest level of water-soluble organic acids, while the events affected by long-range transport from continental East Asia showed high contributions of oxalate to the organic aerosol. Besides, the high-aerosol-loading events had smaller precipitation accumulation than low-aerosol events. Some other Asian studies also indicated that air pollution from China can impact regional weather systems and coupled with convective systems downstream through long-range transport, which intensifies mid-latitude storm tracks and further influence global circulation (Zhang et al., 2007; Li et al., 2008; Wang et al., 2014). Chen et al. (2016) demonstrated the atmospheric transport of SSA from the North Sea to central Europe in detail. They found the influences of SSA indirect effect on nitrate particles can extend to a broader region reaching as far as 400 km from the coast through the "aloft bridge" transport mechanism. Furthermore, previous UK studies suggested that some high pollution episodes are associated with easterly winds and a significant proportion of pollution originated from industrialised parts of continental Europe (King and Dorling, 1997; Stedman, 1998; Buchanan et al., 2002). Because of the large import of inorganic aerosol (OIN) components from mainland Europe, a substantial part of the UK, particularly the south and south-east, is close to or exceeds annual mean limit values (Vieno et al., 2014). Thus, when assessing the impact of aerosols on regional rainfall simulations, it is important to consider not only local aerosols but also externally transported aerosols, especially for some areas with low local anthropogenic emissions.

The influence of aerosol direct and indirect effects has significant seasonal differentiation, which has been highlighted in many meteorological studies. Schultze and Rockel (2018) found a distinct reduction of solar irradiance in long-term aerosol-including simulations over Europe and this reduction is strongest in summer. At the same time, cloud water and ice content decreased over central Europe in summer, reinforcing aerosol absorption and enhancing vertical warming. Another European aerosol study shows that the "Black Triangle" area had obvious changes in both total and light precipitation frequency for directions at which sulphate trends were largest. This trend was also most significant in the summer season (Stjern et al., 2011). In some cases, the seasonality of aerosol impacts is also linked to regional differentiation. According to Cheng et al. (2017), the relationship between aerosol optical depth and cloud effective radius is dominated by the negative correlation over North China in winter and spring and entire China in summer, while the relationship between precipitation and cloud effective radius is dominated by the positive correlation over North China in summer and entire China in autumn. Jiang et al. (2015) investigated the seasonality in anthropogenic aerosol distributions and their effects on clouds and precipitation in East Asia. They summarized that the climate response to anthropogenic aerosols is shown as a northward shift of reduced precipitation, resulting in spring drought in South China and summer drought in North China. In their study, the direct and indirect anthropogenic aerosol effects jointly contributed to spring drought and summer drought was mainly affected by the direct effect. Song et al. (2021) reported a seasonal precipitation delay of 4 to 5 days during 1979–2019 over the northern tropical land and Sahel. Most of the delay was caused by decreased anthropogenic aerosols and increased greenhouse gases that produced more mister atmosphere and enhanced its lag in response to seasonal solar forcing. In particular, these seasonal delays were projected to amplify further in the future decades.

While extensive research has been conducted on the broad-scale impacts of aerosols on global climate and long-term weather patterns, in-depth investigations into the variability of short-lived extreme rainfall events under different conditions remain deficient. Particularly, studies that evaluate the combined impacts of aerosols and seasonal factors on the accuracy of extreme event simulations are limited. Furthermore, a key focus of this study is to compare the performances of the numerical weather prediction (NWP) model with and without aerosol inputs. It tried to figure out whether simulations incorporating aerosol chemistry consistently outperform those based simply on meteorological inputs and under what circumstances this is the case. Given the significant increase in computational demands when including chemical inputs, it is important to understand whether these costs are worthwhile and where shortcomings remain. These knowledge gaps will be filled by conducting a comprehensive analysis of how aerosol properties (mainly particle size and chemical component), transport pathways, and seasonal variations influence the accuracy of WRF-Chem extreme rainfall simulations. In this study, 4-month simulations with aerosol direct and indirect effects and 4-month simulations without aerosol effects over the UK and Ireland were evaluated. The simulation performances of representative rainfall events during the study time were quantitatively evaluated using six metrics and one overall uniform score. The results allow us to assess the model's capability in simulating extreme rainfall frequency, distribution, and intensity under varied chemical and meteorological conditions, thereby enhancing our understanding of aerosol-cloud-precipitation interactions over the UK and Ireland. This study is organized as follows: a description of the used model and observed data are provided in Section 2. The experimental design, study event classification and performance verification method are illustrated in Section 3. Section 4 presents the results and discussion of the impact of aerosol properties, transport and seasonality. Finally, the summary and conclusions of this study are presented in Section 5.

Table 1
WRF-Chem configuration options for the model simulations.

Mode configurations	Description
Model version	WRF-Chem 4.2
Domain size	125 × 125 grid points
Horizontal resolution	10 km × 10 km
Vertical resolution	50 levels up to 50 hPa
Microphysics scheme	MWR
Planetary boundary layer scheme	MYNN2.5
Cumulus scheme	Grell 3D
Longwave radiation scheme	RRTMG
Shortwave radiation scheme	RRTMG
Land surface scheme	Noah Land Surface Model
Surface layer scheme	Nakanishi and Niino PBL's surface layer
Gas-chemistry module	MOZART
Aerosol module	MOSAIC 4 bin
Anthropogenic emissions	EDGARv5.0
Biogenic emissions	MEGAN
Fire emissions	FINNv1.5
Photolysis scheme	New TUV
IC/BC (chemistry)	CAM-chem
IC/BC (meteorology)	ERA5

2. Model and data

2.1. Model description

The rainfall simulations of this study were conducted by the WRF-Chem model version 4.2. Table 1 shows the model configurations briefly. All simulations were configured with one domain (D01) with 10 km horizontal resolutions and 125 × 125 grid points (Fig. 1). The vertical resolution of the model was defined as 50 levels and the top-level pressure is 5000 Pa. These configurations were determined considering the spatiotemporal accuracy and computational efficiency. The European Centre for Medium-Range Weather Forecasts (ECMWF) Global Climate Reanalysis v5 (ERA5; Hersbach et al., 2020) with 0.25° spatial resolution and 1 h temporal resolution was used as initial and lateral boundary conditions (IC/BC) for meteorological parameters. The aerosol radiative effect was simulated by the Morrison 2-moment Morrison (MWR) microphysics scheme (Morrison, Thompson and Tatarskii, 2009) and the Rapid Radiative Transfer Model (RRTMG) scheme (Iacono et al., 2008) for both shortwave and longwave radiation. The Mellor-Yamada Nakanishi and Niino Level 2.5 (MYNN2.5) scheme (Nakanishi and Niino, 2006) was applied for calculating planetary boundary layer height. And Grell 3D (Grell and Dévényi, 2002) was used as the cumulus scheme. The static geographical fields including land use, terrain height, surface albedo, and soil properties were obtained from the Moderate Resolution Imaging Spectroradiometer (MODIS) 21-category data.

Gas phase and aerosol chemistry were based upon the Model for OZone And Related chemical Tracers (MOZART; Emmons et al., 2010) chemistry scheme and the Model for Simulating Aerosol Interactions and Chemistry (MOSAIC; Zaveri et al., 2008) 4 bin aerosol scheme, which also includes aqueous reactions. Emissions Database for Global Atmospheric Research version 5.0 (EDGARv5.0) is used for anthropogenic emissions such as BC, CO, NOx, OC, SO2, PM, NH3 and trace species (Crippa et al., 2020). EDGARv5.0 offers monthly global gridded anthropogenic emission at 0.1∘x0.1∘ resolution for the year 2015 that consists of country-reported emissions and region-specific emissions, which is one of the most recent products that's available. Biogenic emissions from terrestrial ecosystems into the atmosphere are calculated online at 1-km resolution by the Model of Emissions of Gases and Aerosols from Nature (MEGAN; Guenther et al., 2006). Fire INventory from NCAR version 1.5 (FINN1.5) provides daily varying emissions of trace species from biomass burning to the model online plume-rise module (Wiedinmyer et al. 2011). FINN data is derived from daily satellite monitoring of land cover and fires combined with emission factors and estimated fuel loadings. The New TUV photolysis scheme is used for photolytic reactions within MOZART. The Community Atmosphere Model with Chemistry (CAM-chem) provides chemical species to WRF-Chem in every 6-h interval (Buchholz et al., 2019) as chemistry initial and lateral boundary conditions (IC/BC).

2.2. Observational data

For seasonality analysis and simulation accuracy verification, temperature, pressure, relative humidity, water vapor mixing ratio, wind

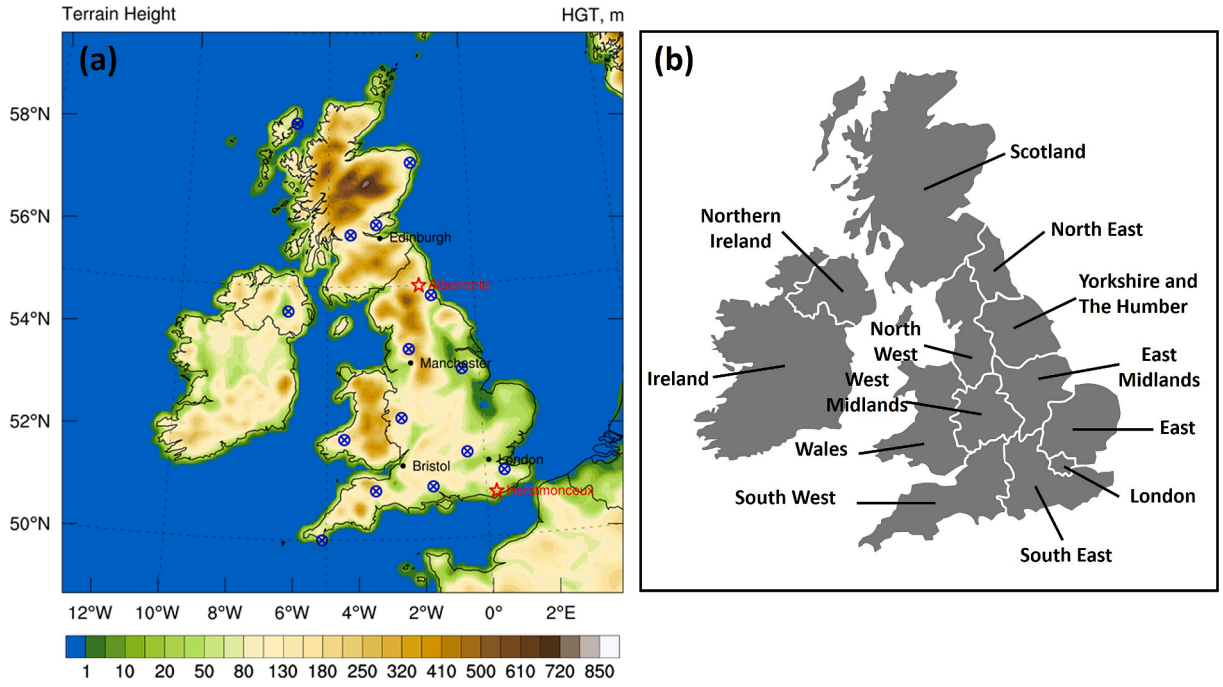

Fig. 1. Computational domain for rainfall simulations in the UK and Ireland. (a) Locations of surface meteorological observations. The red five-pointed stars represent two Met Office stations that provide radiosonde data. The blue circles with a cross in the centre represent 15C-band rainfall radars. (b) Map of the regions making up the study area. (For interpretation of the references to colour in this figure legend, the reader is referred to the web version of this article.)

Table 2
Criteria used to classify HYSPLIT backward trajectory transport patterns for rainfall events.

Category	Description of trajectory categories
AT	Trajectory originating in the Northern Atlantic Ocean during the backward 5-day period.
AR	Trajectories originating in areas within or near the Arctic, primarily Iceland, Greenland and the Canadian Arctic Archipelago, during the backward 5-day period.
WE	Trajectory originating in or crossing Western Europe (i.e. area west of the Netherlands) during the backward 5-day period.
CE	Trajectory originating in or crossing Central Europe (i.e. area east of the Netherlands) during the backward 5-day period.
NE	Trajectory originating in or crossing Northern Europe (i.e. area north of the Demark) during the backward 5-day period.

speed and rainfall data from ground and satellite observations were used.

2.2.1. AIRS data

The Atmospheric Infrared Sounder (AIRS) is a high-resolution infrared spectrometer onboard NASA's Earth Observing System Aqua satellite. This product was divided into ascending (1:30 PM local time) and descending (1:30 AM local time) observations. As we are interested in the monthly values, the ascending and descending data were averaged. Specifically, this study used AIRS version 7.0 level 3 monthly skin temperature (SurfSkinTemp_A and SurfSkinTemp_D) and surface pressure (SurfPres_A and SurfPres_D) data available at $1^\circ \times 1^\circ$ grid cells (AIRS project, 2019). AIRS provides retrievals at 100 vertical levels with a nominal accuracy of 1 K/km for temperature, which has been validated by some studies using aircraft and in situ observations (e.g., Divakarla et al., 2006).

2.2.2. Radiosonde data

This study compared the vertical profiles of pressure, temperature, humidity mixing ratio, relative humidity, and wind speed over two Met Office stations in the UK (Albemarle and Herstmonceux) from radiosonde observations with model simulated vertical profiles (Met Office, 2007a, Met Office, 2007b). The high-resolution radiosonde data were provided by the Met Office, with a measurement interval of 2 s and the ascents extend to heights of about 20–30 km. All available data were averaged to estimate the monthly profile and compared with simulations. The locations of the two Met Office stations in the UK that provide radiosonde data are shown by the red five-pointed stars in Fig. 1.

2.2.3. NIMROD radar dataset

The radar rainfall estimates adopted in this study came from the UK NIMROD composite dataset, which was collected and processed by the Met Office through a network of 15C-band rainfall radars. The locations of these 15C-band rainfall radars are represented in Fig. 1 by blue circles with a cross in the centre. The rainfall rate analysis used processed radar and satellite data along with ground reports and NWP fields. Data are available from 2004 until the present with spatial and temporal resolutions of 1 km and 15 min (Met Office, 2003). This dataset has also been adjusted by rain gauge measurements and extensive processing to correct the various radar errors like clutter, noise, attenuation, occultation, bright band, geographic enhancement and anomalous propagation, etc (Harrison et al., 2000). Thus, NIMROD high-resolution radar rainfall estimates incorporate the latest processing algorithms of Met Office and stand as one of the best rainfall estimates in the UK suitable for rainfall simulation validations.

3. Method

3.1. Experimental design

In this study, four seasons (with one month each) in 2020: February (winter), May (spring), August (summer) and October (autumn) were selected as the study periods. The representative months for each season are determined based on when most extreme rainfall events occur. During these 4 months, a total of 12 significant rainfall events occurred under various meteorological and aerosol conditions. To evaluate the impact of aerosol properties, transport and seasonality on rainfall simulations in the UK and Ireland, this study was carried out in three main steps. Firstly, two sets of simulations were conducted by the WRF-Chem model in this study, i.e., baseline simulations (WB) that with chemistry and provide aerosols as output but both direct and indirect aerosol effects turned off, and simulations that fully consider aerosol direct and indirect effects (WDAIE) with scavenging and cloud chemistry turned on. AIRS satellite, radiosonde and NIMROD radar data were used to compare with WDAIE and WB results to understand meteorological differences (i.e. surface temperature, surface pressure, water vapor mixing ratio, RH, wind speed and rainfall) during different seasons in the UK and Ireland and verify the reliability of the simulations. The particle mass distribution (PMSD) of each compound in different seasons from WDAIE and WB simulations was also compared. Next, the Hybrid Single-Particle Lagrangian Integrated Trajectory (HYSPLIT) model from NOAA (Stein et al., 2015) was used to run the back trajectory of each event and derive its aerosol transport source. In addition, by examining the variations in aerosol mass (including Na, Cl, SO_4, NO_3, NH_4, BC, OC, and OIN) over time at different vertical levels and their correlation with the changes in rainfall, it is possible to identify the key aerosol components that contribute to the rainfall. Finally, WB and WDAIE simulation performances were quantified using a verification method consisting of six metrics and an overall performance score. Based on the analysis in previous steps, the ranking and improvement of simulation performances were discussed in relation to the impacts of aerosol properties, transport and seasonality. The Probability Density Function (PDF) and Taylor diagram of rainfall for each event were also presented to help

Table 3
The detailed information and trajectory categories of 12 study events.

Month (Season)	Name	Date and duration	Trajectory categories	Event brief description
February (Winter)	Event 1	8–9 Feb (36 h)	AR(CE,WE)	Storm Ciara
	Event 2	15–16 Feb (36 h)	AT	Storm Dennis
	Event 3	28–29 Feb (36 h)	AR	Storm Jorge
May (Spring)	Event 4	21–23 May (48 h)	AT(WE)	Highland rainfall
August (Summer)	Event 5	3–6 Aug (60 h)	AR	Extreme Scotland rainfall
	Event 6	12–16 Aug (96 h)	CE	Norfolk rainfall
	Event 7	19–22 Aug (72 h)	AT	Storm Ellen
	Event 8	24–26 Aug (36 h)	AR	Storm Francis
October (Autumn)	Event 9	2–5 Oct (60 h)	AR(WE)	Storm Alex
	Event 10	7–8 Oct (24 h)	AR	Wales rainfall
	Event 11	18–22 Oct (84 h)	AR	Extreme Highland rainfall
	Event 12	31 Oct (24 h)	AR	Storm Aiden

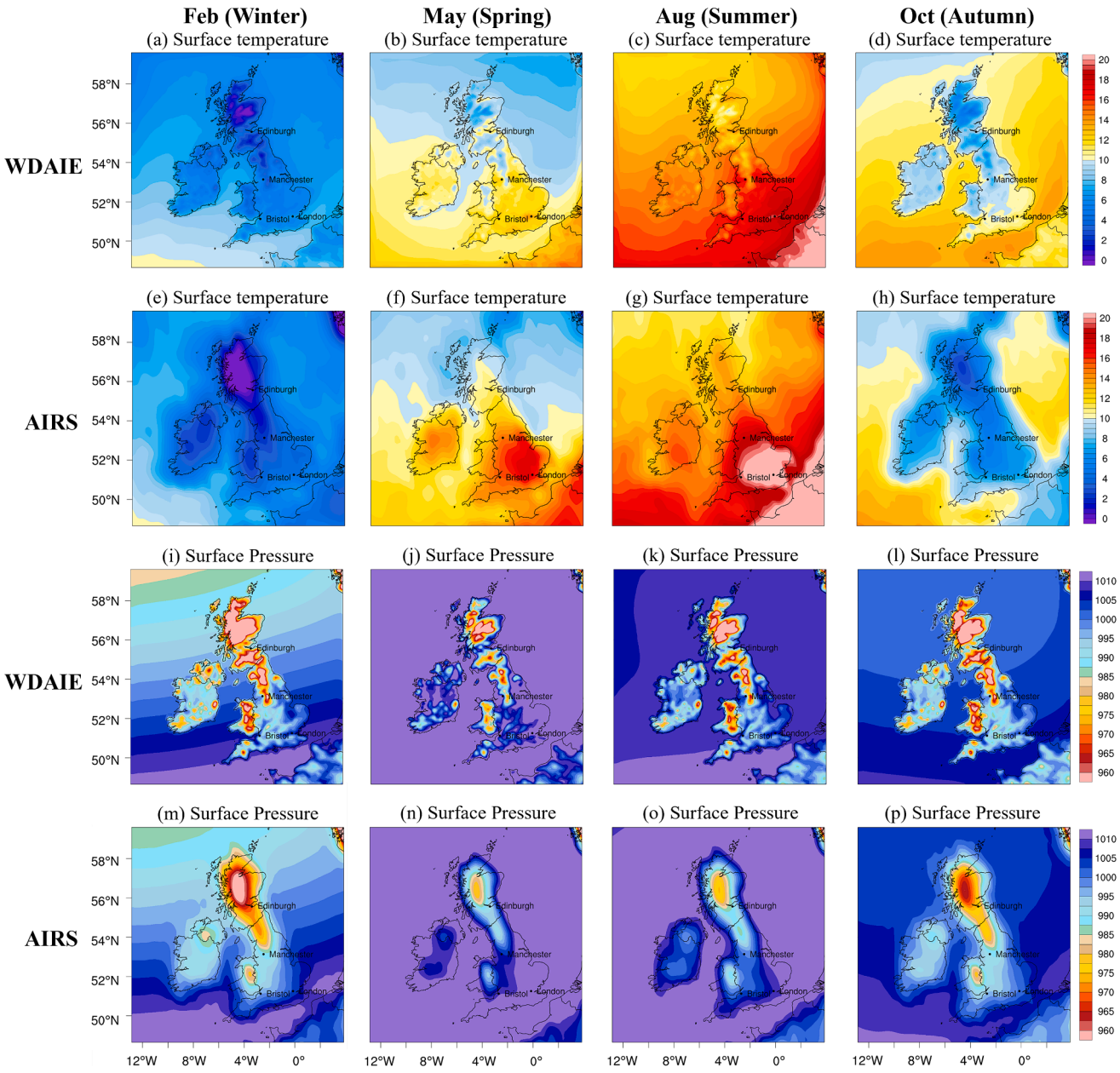

Fig. 2. Monthly average (a-h) surface temperature and (i-p) surface pressure for February, May, August and October 2020 from WDAIE simulations and AIRS observations.

understand the reasons for performance variability. A detailed description of back trajectory production and performance verification method are shown in the following sections.

3.2. *Trajectory classification*

Air mass back trajectories can provide information about the source of air pollutants, which is useful for investigating the relationships between aerosol and extreme weather. NOAA's HYSPLIT model has been widely used in global studies to investigate aerosol transport in different regions and has received positive feedback for its effectiveness (e.g., Escudero et al., 2006; Kumar et al., 2014; Stein et al., 2015; Braun et al., 2020). Considering atmospheric aerosols' average life span of about 5 days, the HYSPLIT model was forced to run for 120 hr using the Global Data Assimilation System (GDAS, 1° spatial resolution) gridded meteorological reanalysis dataset for backward trajectories generation of extreme rainfall events. To demonstrate the long-range transport of aerosols during rainfall formation, each event contains 24 backward trajectories initialized at 100 m above sea level from the beginning of rainfall and centred on its maximum accumulated rainfall point. These model parameters were determined based on previous studies on long-distance aerosol transport (Rai et al., 2022; He et al., 2020; Wang et al., 2016). The backward trajectories corresponding to 12 rainfall events can be found in Fig. S1 and Fig. S2 in the Supplement. According to the trajectory results, trajectories were assigned to five categories using the criteria in Table 2: Atlantic Ocean (AT); Arctic (AR); Western Europe (WE); Central Europe (NE) and Northern Europe (NE). The detailed information and trajectory categories of the 12 rainfall events included in the 4-month simulations of WDAIE and WB are shown in Table 3. The trajectory classification mainly shows the source of the aerosols. However, some trajectories pass through multiple regions, which are marked in parentheses to help the subsequent discussion.

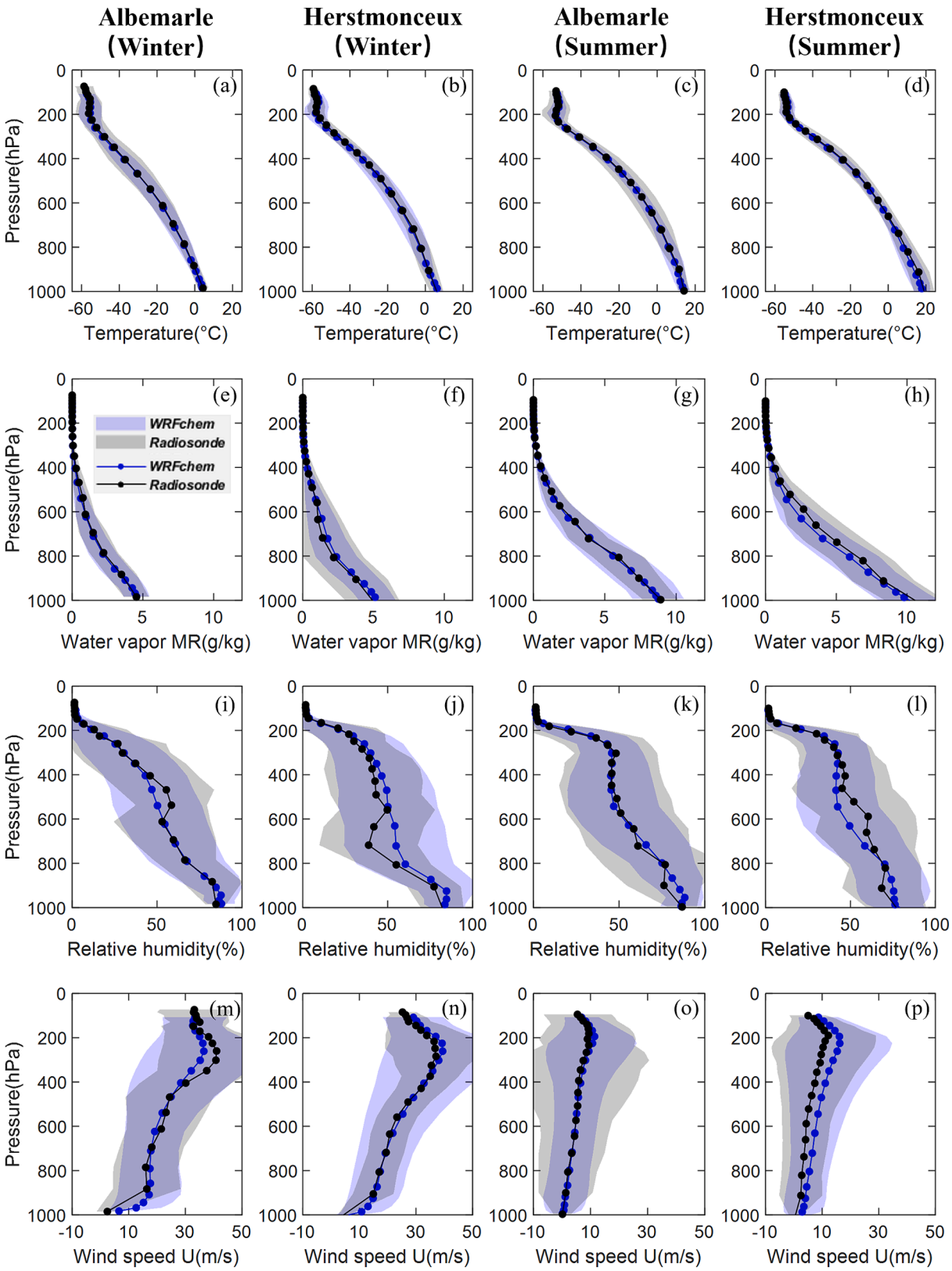

Fig. 3. Vertical profile of (a, b, c, d) temperature (℃), (e, f, g, h) water vapor mixing ratio (g/kg), (i, j, k, l) relative humidity (%), and (m, n, o, p) wind speed (m/s) over Albemarle and Herstmonceux in winter and summer from WDAIE simulations and radiosonde observations.

3.3. Performance verification

To evaluate the spatiotemporal performance of simulations under different conditions, this study uses six metrics and one overall performance score to quantify WDAIE and WB simulations with respect to the NIMROD radar dataset. Six metrics include the Probability of Detection (*POD*), the False Alarm Ratio (*FAR*), the Frequency Bias Index (*FBI*), the Critical Success Index (*CSI*), the Root Mean Square Error (*RMSE*) and the

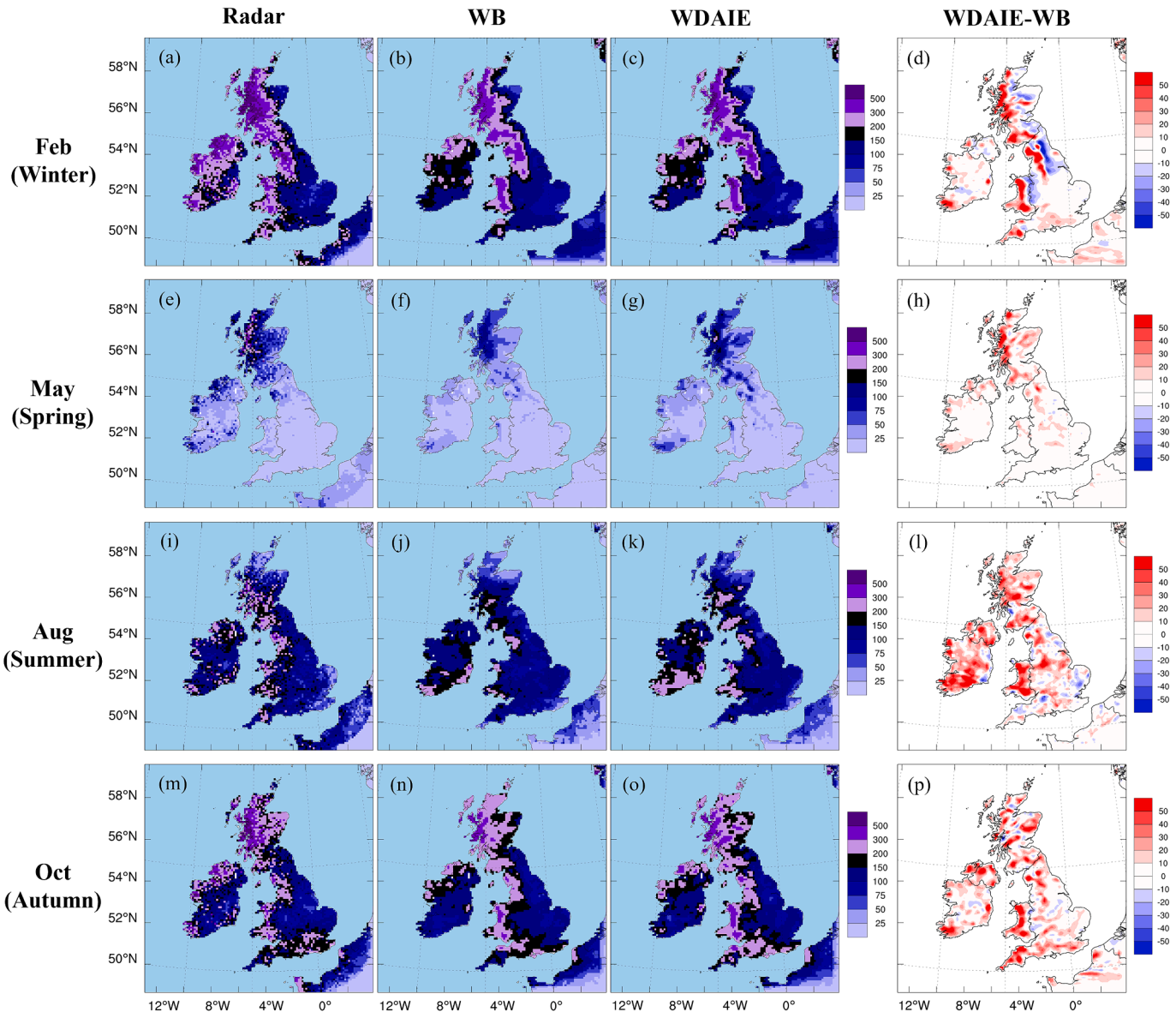

Fig. 4. Monthly accumulated rainfall map from (a, e, i, m) radar observations, (b, f, j, n) WB simulations and (e, g, k, o) WDAIE simulations for February, May, August and October 2020, respectively. (d, h, l, p) spatial map of difference in rainfall pattern simulated by WRF-Chem model with and without aerosol effects (WDAIE-WB).

Correlation coefficient (*R*). The first four metrics represent the probability of detecting rainfall and generating false rainfall, the tendency to overestimate or underestimate rainfall, and the critical performance, respectively. The calculation of these error metrics is according to the rainfall contingency table, as shown in Table S1 in the Supplement. RR, NR, RN and NN represent the grid numbers of hits, misses, false alarms and correct negatives, respectively. Besides, RMSE shows the difference between model predictions and observations and R measures the strength and direction of the linear relationship between predicted and observed rainfall. These six metrics provide a comprehensive framework for evaluating the performance of rainfall simulations, covering aspects from probability detection to error analysis and trend correlation. The metric values can be calculated through Equations (1)-(6) in the Supplements. In the equations, i and N refer to each time step and the total time step of the whole event, while j and M refer to each rainfall grid and the total number of grids. S_{ij} and O_{ij} are the simulated and observed rainfall accumulations at each time step i and rain grid j, and $\overline{S}_i$ and $\overline{O}_i$ are the means of the values of the simulated and observed at each time step i. Considering a suitable threshold may help investigate the accuracy of simulations, the grids with rainfall below 0.1 mm are removed when calculating metric values. The six metrics are calculated by interpolating the NIMROD radar dataset to the WDAIE and WB simulations' grid at a 12-hour time step in D01.

Because each metric represents a different type of performance characteristic, it is difficult to determine how overall simulation performance changes with the impacts of aerosol properties, transport and seasonality. To uniformly quantify the results of six metrics, The Relative Closeness Value of Technique for Order of Preference by Similarity to Ideal Solution (*TOPSIS RCV*) proposed by Hwang and Yoon (1981) is applied to evaluate the overall performance of each simulation in this study. This method has also been further developed and used by Liu et al. (2021) and Liu et al. (2023). To obtain a uniform score where 0 indicates the poorest performance and 1 the best, all six metrics are rescaled to a range between 0 and 1 and given equal weight in the computation of the *TOPSIS RCV*. Thus, the possible range of this overall score would be 0–1 and the perfect value is 1. By this way, *TOPSIS RCV* could easily show the overall performance differences and improvements of simulations under different meteorological conditions. The

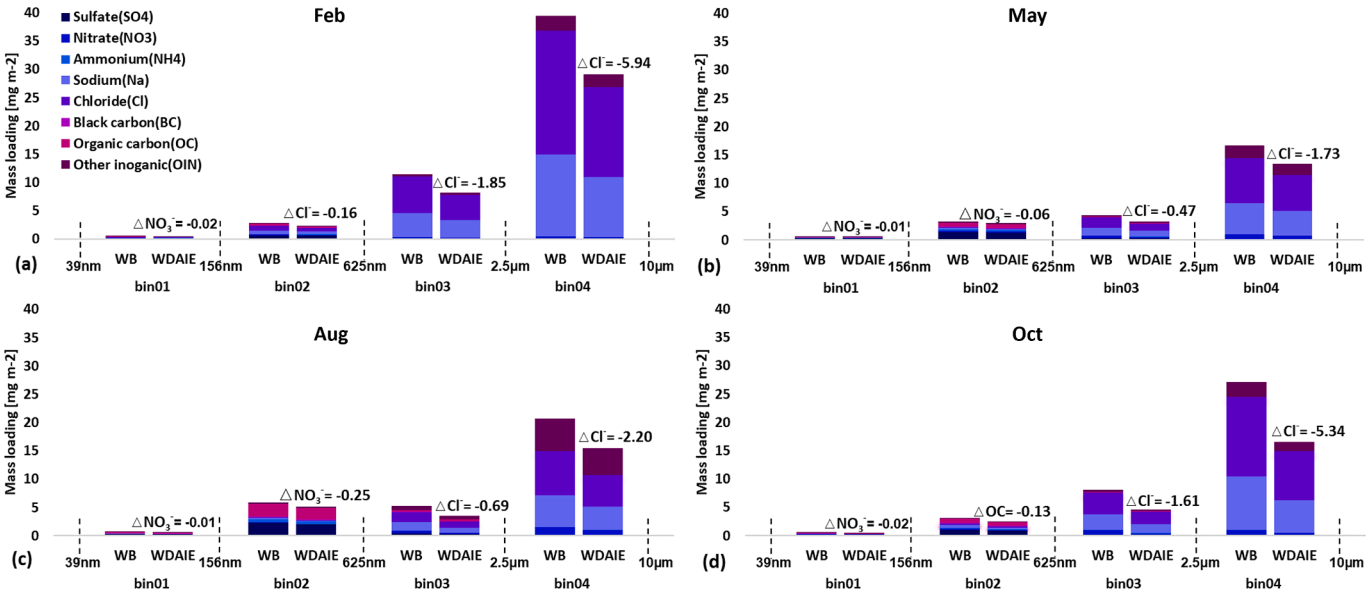

Fig. 5. Particle mass size distribution (PMSD) for each chemical compound over the study domain from WDAIE and WB simulations. (a-d) PMSD results in February, May, August and October 2020, respectively. The maximum difference of component PMSD between the WB and the WDAIE for each bin is marked.

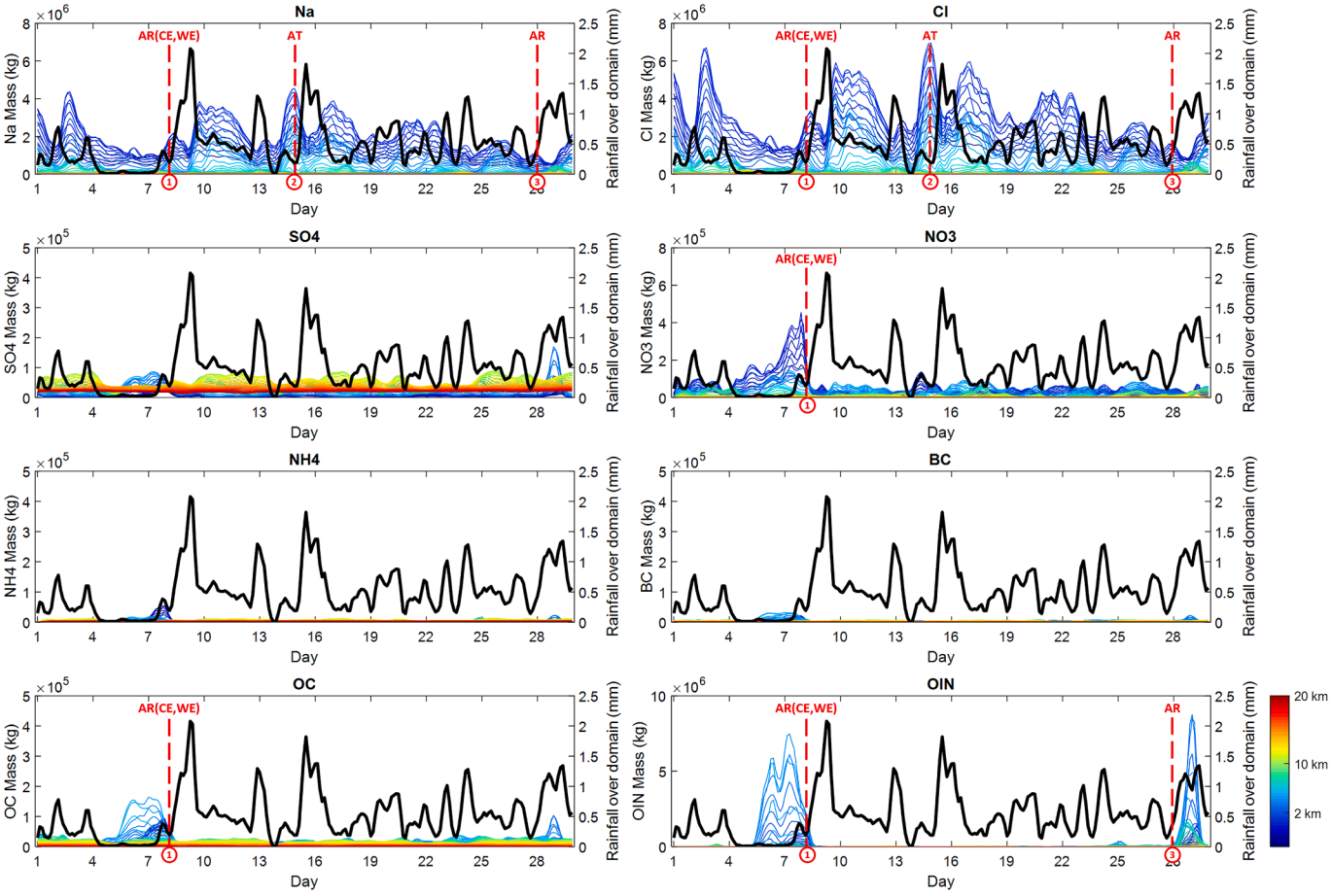

Fig. 6. Mass variations of different aerosols (Na, Cl, SO4, NO3, NH4, BC, OC and OIN) over time at different vertical levels in February. Black lines represent the change in average rainfall (mm) over the domain. Coloured lines from blue to red represent changes in aerosol mass over time from the near-surface to the upper atmosphere levels. The positions of the vertical red dashed lines with number and text labels indicate the onsets of rainfall events. The numbers are the sequence of events and the texts indicate the origins of the air masses for events. For example, Event 1 with the label "AR (CE, WE)" indicates that the air mass of this event originated in AR and passed through CE and WE (Table 2). (For interpretation of the references to colour in this figure legend, the reader is referred to the web version of this article.)

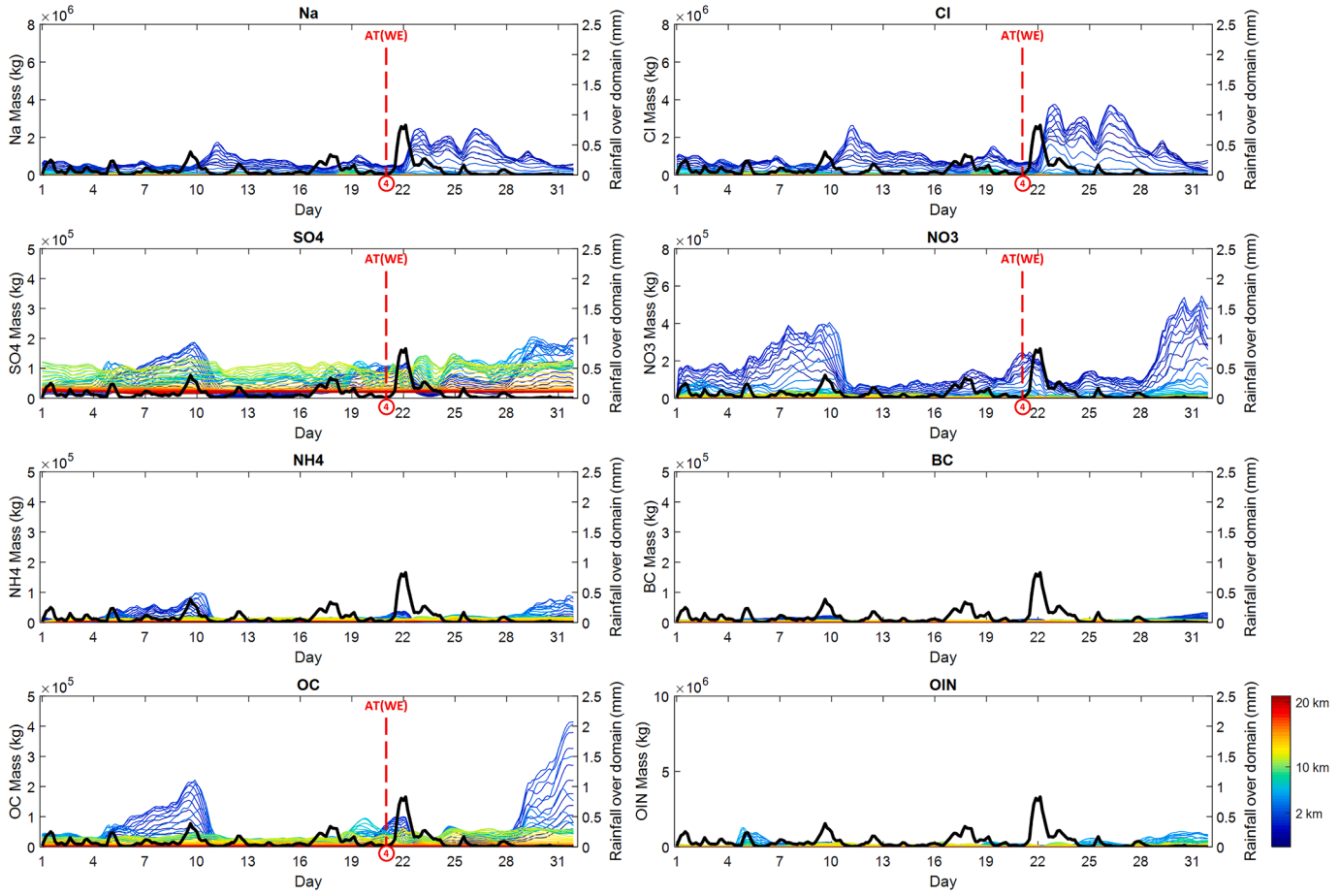

Fig. 7. Similar to Fig. 6, but for the mass variations of different aerosols over time at different vertical levels in May.

detailed score calculation method and conversion between the original and rescaled metrics can be found in Equation (7) and Table S2 in the Supplement.

4. Results and discussions

4.1. Meteorological seasonality evaluation

Meteorological conditions play an important role in the spatial and temporal distribution of aerosols by facilitating their transport, scavenging or deposition, and mixing in the atmosphere (Kaufman et al., 2002). Therefore, accurate meteorological variables are crucial to simulating aerosol-cloud-precipitation-meteorology interactions and estimating the impact of aerosols. Fig. 2 (a-d) and (i-l) display the spatial distribution of WDAIE simulated monthly averaged temperature and pressure at the surface for different seasons. These meteorological parameters are compared and evaluated by AIRS satellite data in Fig. 2 (e-h) and (m-p). In addition, model simulated and radiosonde observed vertical profiles of temperature, water vapor mixing ratio (MR), RH and wind speed were compared at two Met Office stations of the UK named Albemarle and Herstmonceux (Fig. 3). Due to data availability, only winter and summer radiosonde results are presented. The results show that simulations successfully capture the broad meteorological characteristics of the study area.

Using the winter surface temperature as a baseline, the temperature in the same region rises approximately 7 degrees in spring, 10 degrees in summer, and 5 degrees in autumn. The surface temperature is usually low over Scotland due to high elevation and also because this is one of the major rainfall areas of the UK. In contrast, the high temperature is observed over South East and East of England as these areas usually receive less rainfall. Compared to AIRS observations, the temperature gradient of WDAIE simulations appears more refined and the regions experiencing temperature extremes (above 20 °C or below 0 °C) become smaller. Regarding surface pressure, the study area experiences stable high pressure during spring and summer, contrasted with relatively unstable low pressure in winter and autumn. Surface pressure results from AIRS observations seem much blurred in contrast to WDAIE simulations while pressure results over the sea are almost the same. As for vertical parameters, it is observed that monthly averaged temperature, RH, water vapor MR and wind speed profiles are simulated reasonably well by the WRF-Chem over two locations (Fig. 3). At all the heights, the model simulated data and radiosonde data are in the same range within variation. In general, all meteorological parameters from surface to vertical layers are simulated well in the WDAIE simulations. Some differences between the simulations and observations can be attributed to the difference in spatial resolution (WDAIE is at 10 km resolution, while AIRS is at 1 degree resolution), temporal difference (WDAIE is available 3 hourly, AIRS and radiosonde data are available daily), and also because of uncertainty arising from model simulations and observation process.

Monthly accumulated rainfall distributions from WDAIE and WB simulations for different seasons were also evaluated against NIMROD composite dataset. Overall, the simulations are consistent with radar observations in terms of rainfall distribution but with lower rainfall intensity. The rainfall in winter and autumn of 2020 is significantly greater than in spring and summer, and the highest monthly rainfall in some areas is more than 500 mm. Besides, most of the heavy rains are concentrated in Scotland, Wales, North West and South West of England (Fig. 1 (b)). Firstly, the regions experiencing frequent extreme rainfall are all at high elevations, as illustrated in Fig. 1 (a). When air masses

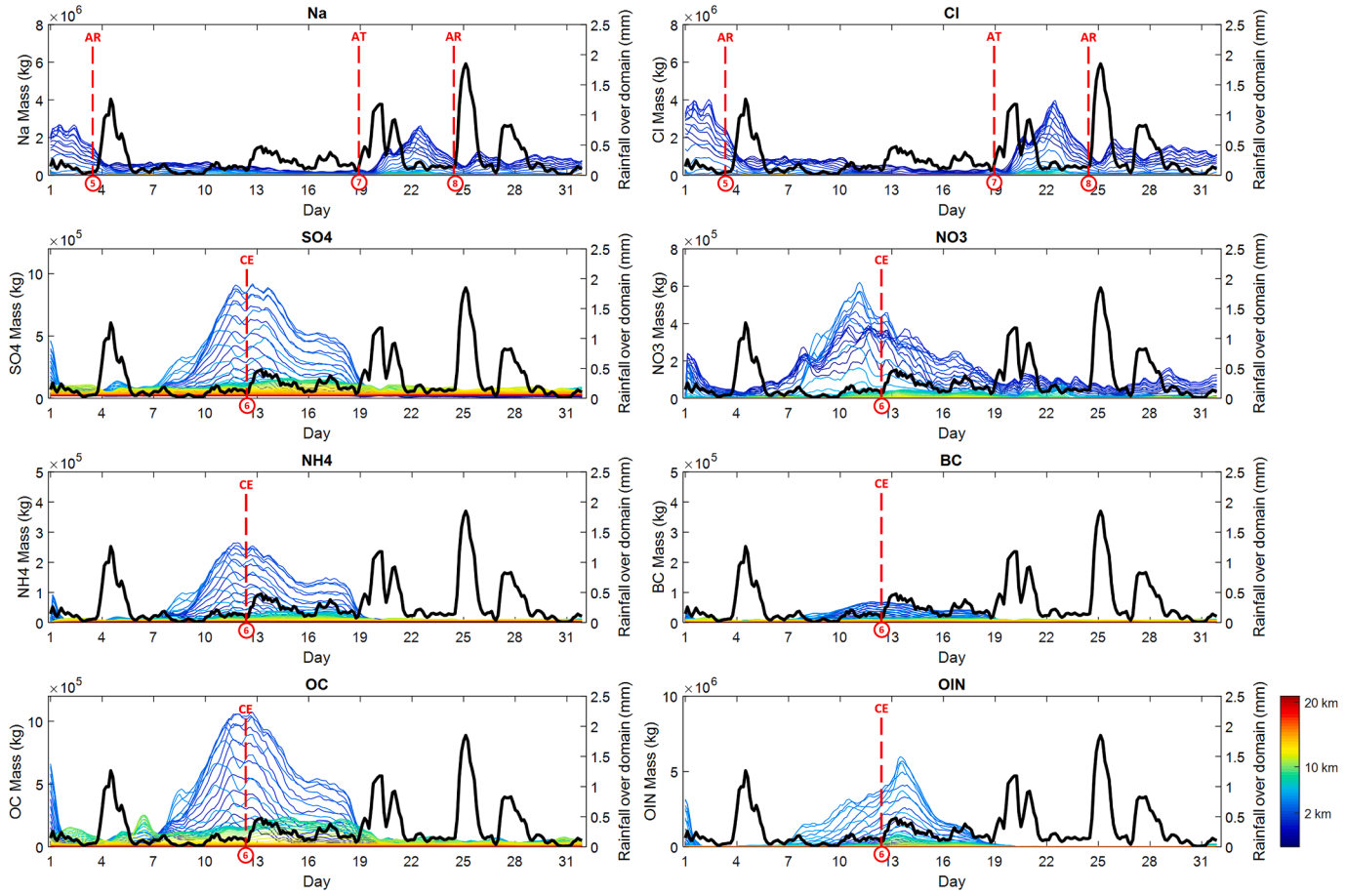

Fig. 8. Similar to Fig. 6, but for the mass variations of different aerosols over time at different vertical levels in Auguest.

encounter a topographical barrier, significant precipitation may be accumulated within a narrow region (Sumner, 1988), this phenomenon is known as the "orographic enhancement effect". Next, the UK's unique geographical location makes its weather susceptible to the influence of moist air masses from the North Atlantic Ocean. Some studies pointed out that the heaviest orographic precipitation in the UK has long been associated with strong southwest and west winds in the warm, moist sectors of frontal depressions (Browning et al., 1974; Douglas and Glasspoole, 1947). Therefore, the direction and source of aerosol transport are also important factors to be explored in this study. Fig. 4 (d, h, l, p) shows the difference in monthly rainfall when the aerosol contribution is included (WDAIE) and removed (WB) in model simulations. It is found that aerosol direct and indirect effects increased rainfall in spring, summer and autumn. But in winter, the aerosol effect plays an adjustment role in rainfall patterns, causing the location of some rainfall to shift westward (moving from the blue area to the red area in Fig. 4 (d)). Subsequent sections will further discuss the various impacts of aerosols from the perspective of extreme rainfall events.

4.2. Aerosol properties and transport evaluation

To explore the properties of size-resolved aerosol particles, the fully coupled sectional aerosol module MOSAIC was used in WRF-Chem simulations. In MOSAIC, particles are assumed to be internally mixed in each bin (Zaveri et al., 2008). Dry particles are categorized into four discrete size bins, ranging approximately from 39 nm to 10 μm, as shown in Fig. 5. In order to know the influence of aerosol effects on each component PMSD, the PMSD of WB and WDAIE simulations during different seasons were calculated over the study domain. It is obvious that there is a higher aerosol mass loading over the study area in February (winter) and October (autumn) simulations and most of the total amount is contributed by Na and Cl. Simulations in August (summer) have unusually high SO_4, OC and OIN loading compared to other months, which may have been transported from outside the study domain. When aerosol effects are considered, the total aerosol mass in every size bin significantly decreases due to aerosol participation in rainfall and rainfall washout. Furthermore, Cl reduces mostly in the larger size bins (bins 03–04) for each season, while NO_3 reduces mostly in the smaller size bin (bin 01) but with much smaller magnitude.

In addition to exploring aerosol seasonal changes in different particle sizes, aerosol spatiotemporal changes during different rainfall events are also investigated in this study (Figs. 6-9). Figs. 6-9 show the mass variations of Na, Cl, SO_4, NO_3, NH_4, BC, OC and OIN over time at different vertical levels in February, May, August and October, respectively. The black lines in these figures show the change in average rainfall over the domain to better visualize the relationship between aerosols and rainfall. The coloured lines represent aerosol mass changes over time from the near-surface to the upper atmosphere (approximately 0–20 km above the surface). Since the growth of cloud droplets and the formation of rainfall can involve the entire vertical range of clouds and the height of clouds can range from a few hundred meters to several kilometres above the ground, aerosols with a vertical height below 10 km are defined as the primarily participating aerosols in the generation of rainfall. Among them, dark blue, light blue and some green lines represent the aerosol changes below 10 km. Besides, the vertical red dashed lines are used to show the start point of every rainfall event, which are also labelled with the event sequence numbers and transport trajectory categories. The detailed description of rainfall events and transport trajectory categories can be found in Section 3.2, Table 2 and Table 3. In order to summarize the aerosols associated with each rainfall

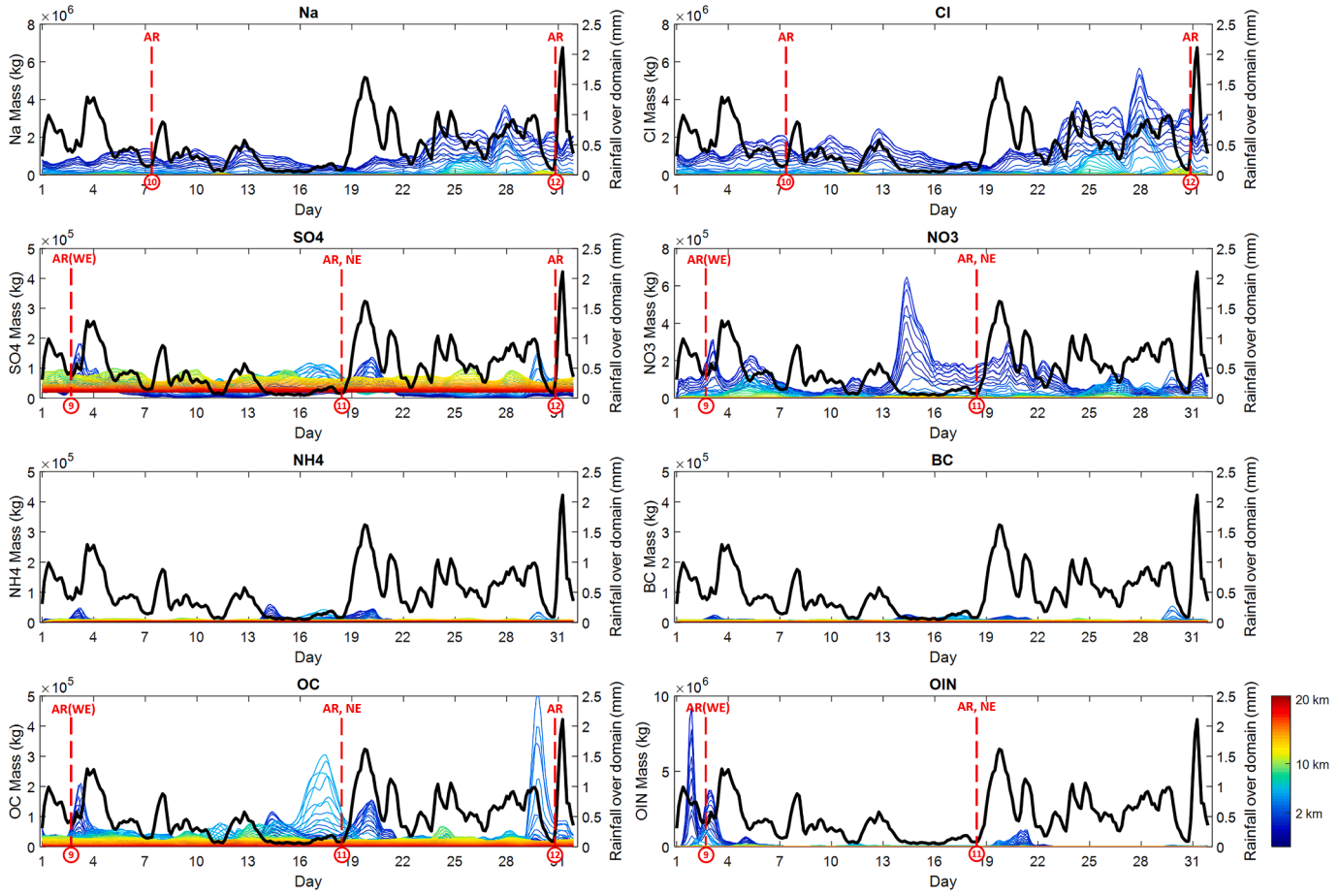

Fig. 9. Similar to Fig. 6, but for the mass variations of different aerosols over time at different vertical levels in October.

event generation, aerosol components with significant mass fluctuations (greater than or equal to 50 % of the average) before and during events are defined as "Dominant aerosol components". At the same time, the sources of the air mass also need to be considered to determine the reasonability of the dominant aerosol components.

Taking Event 1 in February as an example, the red dashed lines with label 1 were added to the Na, Cl, NO_3, OC, and OIN subfigures to illustrate that these types of aerosols dominate and promote rainfall (Fig. 6). The label "AR (CE, WE)" indicates that the air mass of this event originated in AR and passed through CE and WE. Event 3 also originated in AR but only involved Na, Cl, and OIN. This may be because its trajectory only spanned from the Canadian Arctic Islands to the UK and did not pass through some of Europe's high-emission countries. In contrast to the two AR events, the air mass in Event 2 originated from the North Atlantic Ocean and resulted in large amounts of Na and Cl transport that produced rainfall. The spring of 2020 in the UK was particularly dry, with only one significant local rainfall occurring in the Highlands on 21 May (Event 4 of Fig. 7). Under the influence of dry weather conditions and high-pressure systems (Fig. 2), the mechanisms for aerosol removal by rainfall and aerosol vertical dispersion were weakened, leading to a noticeable increase in the concentrations of SO_4 and NO_3 in the lower to mid-atmosphere compared to February. However, the atmospheric circulation patterns in spring resulted in a reduction of moist airflow from the Northern Atlantic Ocean, simultaneously decreasing the transport of sea salt aerosols Na and Cl. According to the trajectory categories, the air mass of Event 4 originated in AT passing through WE and mainly involved Na, Cl, SO_4, NO_3, and OC. Unlike events that originated in AT and AR, a particular rainfall event (Event 6) prompted by the air mass originating from Central Europe (CE) occurred in August. This air mass contained high concentrations of pollutants far exceeding those in the

Table 4
Simulation performance results and related impact information for rainfall events ranked based on WDAIE overall scores.

Name	WDAIE scores	WB scores	Month	Trajectory categories	Dominant aerosol components
Event 3	0.891	0.886	Feb	AR	Na, Cl, OIN
Event 10	0.875	0.886	Oct	AR	Na, Cl
Event 2	0.863	0.855	Feb	AT	Na, Cl
Event 1	0.838	0.819	Feb	AR(CE,WE)	Na, Cl, NO_3, OC, OIN
Event 9	0.823	0.825	Oct	AR(WE)	SO_4, NO_3, OC, OIN
Event 8	0.819	0.828	Aug	AR	Na, Cl
Event 12	0.805	0.788	Oct	AR	Na, Cl, SO_4, OC
Event 11	0.781	0.787	Oct	AR, NE	SO_4, NO_3, OC, OIN
Event 7	0.775	0.775	Aug	AT	Na, Cl
Event 5	0.744	0.744	Aug	AR	Na, Cl
Event 4	0.683	0.676	May	AT(WE)	Na, Cl, SO_4, NO_3, OC
Event 6	0.446	0.480	Aug	CE	SO_4, NO_3, NH_4, BC, OC, OIN

Table 5
Simulation performance results and related impact information for rainfall events ranked based on overall score improvements.

Name	Score improvement	Peak accumulated grid rainfall (mm)	Month	Trajectory categories	Dominant aerosol components
Event 1	2.3 %	136.741	Feb	AR(CE,WE)	Na, Cl, NO_3, OC, OIN
Event 12	2.2 %	156.038	Oct	AR	Na, Cl, SO_4, OC
Event 4	1.0 %	199.638	May	AT(WE)	Na, Cl, SO_4, NO_3, OC
Event 2	0.9 %	129.736	Feb	AT	Na, Cl
Event 3	0.6 %	91.505	Feb	AR	Na, Cl, OIN
Event 5	0.0 %	183.206	Aug	AR	Na, Cl
Event 7	0.0 %	206.12	Aug	AT	Na, Cl
Event 9	-0.2 %	157.783	Oct	AR(WE)	SO_4, NO_3, OC, OIN
Event 11	-0.8 %	364.982	Oct	AR, NE	SO_4, NO_3, OC, OIN
Event 8	-1.1 %	118.71	Aug	AR	Na, Cl
Event 10	-1.3 %	57.6001	Oct	AR	Na, Cl
Event 6	-7.1 %	167.001	Aug	CE	SO_4, NO_3, NH_4, BC, OC, OIN

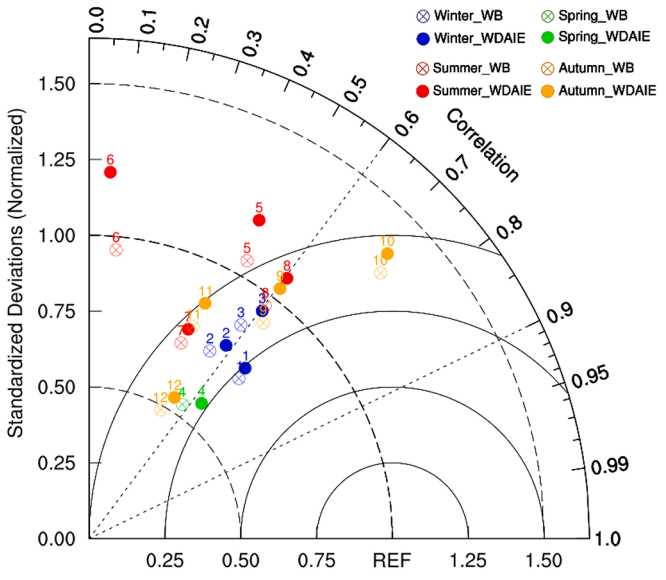

Fig. 10. Taylor diagram of rainfall for Events 1–12. Blue, green, red and orange dots represent winter, spring, summer and autumn rainfall events respectively. The solid dots are WDAIE simulations, while circles with a cross in the centre are WB simulations. (For interpretation of the references to colour in this figure legend, the reader is referred to the web version of this article.)

UK, including SO_4, NO_3, NH_4, BC, OC and OIN, which caused a surge in these aerosols between August 7–19 in the study domain (Fig. 8) and then facilitated persistent thunderstorms in the southern UK and Ireland with widespread rainfall. Furthermore, the dominant aerosol components of Event 6 were identified as not containing Na and Cl due to the low concentration and no obvious change in SSA during the event. As for events 5, 7 and 8, they are similar to previous AR or AT events, dominated by Na and Cl aerosols but occurred under different seasonal conditions. The four rainfall events in October all originated from AR but presented different characteristics. Most of Event 9 air mass came from Greenland and crossed WE, carrying some SO_4 and NO_3 aerosols along the way to the UK. According to the aerosol spatiotemporal variation, OIN aerosol may play the most important role in this rainfall, followed by NO_3, OC and SO_4. Compared to other events, the rainfall coverage and intensity of Event 10 were smaller with Na and Cl being the primary aerosol components contributing to its development. The trajectory category of Event 11 is difficult to determine because the event's back trajectory circled over the ocean between Iceland and Northern Europe for 5 days (Fig. S2 in the Supplement). Thus, it is labelled as "AR, NE" to indicate its origin. Analysis based on Fig. 9, this rainfall occurred when the SSA concentration was relatively low and the primarily involved aerosols may be NO_3, SO_3, OC and OIN. In contrast, Na and Cl aerosol concentrations during Event 12 were much higher and fluctuated greatly. OC and SO_4 aerosol also seem to contribute to the rainfall of Event 12. The backward trajectories of these 12 events can be seen in Fig. S1 and Fig. S2 of the Supplement. The dominant aerosol components identified here as drivers for each event will be discussed in connection with the simulation performance of rainfall events in the following section.

4.3. *Impacts on rainfall simulation performance*

To better analyse the impact of aerosol properties, transport and seasonality on rainfall event performance, the overall scores of the WB and WDAIE simulations were used to identify their differences and improvements. The overall score is a comprehensive score calculated based on the results of *POD, FBI, CSI, FAR, RMSE* and *R* metrics, which can show the overall spatiotemporal performance and facilitate comparison between simulations. The values of the overall score and six metrics for 12 events are shown in Table S3 of the Supplement. Table 4 shows the simulation performance results and related impact information for rainfall events ranked according to WDAIE overall scores. Table 5 displays the improvements ((WDAIE-WB)/WB) of overall performance for rainfall events when the aerosol direct and indirect effects are included in rainfall simulations. The Taylor diagram for events in different seasons is presented in Fig. 10. The Probability Density Functions (PDF) of rainfall derived from WDAIE, WB and radar observations are illustrated in Fig. 11 to help understand the distribution and likelihood of different rainfall intensities during the events. The accumulated rainfall maps for the best-performing event in WDAIE simulations, the worst-performing event in WDAIE simulations and the most-improved event are presented in Fig. 12.

As shown in Table 4, it is obvious that the rainfall simulation performances of events in February and October are better than those in August and May. In the UK, rainfall patterns can vary significantly across different seasons, but generally winter and autumn are the seasons with more storms and rainfall. This is due to the UK's geographical position making it susceptible to Atlantic depressions during these seasons. There is a total of 7 storms among the 12 study events and most of their simulation performances are better than other thunderstorms or localized rainfall. In particular, the WDAIE simulations of five winter and autumn storms (Event 1, 2, 3, 9, 12) performed very well, ranking 4th, 3rd, 1st, 5th, and 7th respectively. In contrast, spring and summer are less influenced by Atlantic depressions and tend to be drier, although summer can sometimes experience heavy rainfall during thunderstorms. The model simulations of events in August and May did not achieve satisfactory results and 4 of the 5 events ranked last. Among them, the overall scores of two storm events (Events 7 and 8) are higher than the other three rainfall events. Besides, Fig. 10 is a Taylor diagram of rainfall events in different seasons. Based on standardized deviations and correlation, the simulations in winter (blue dots) also outperform the simulations in the other three seasons. From the perspective of aerosol properties in Table 4, the model's ability to simulate rainfall mainly promoted by sea salt aerosols (Na and Cl) is greater than rainfall

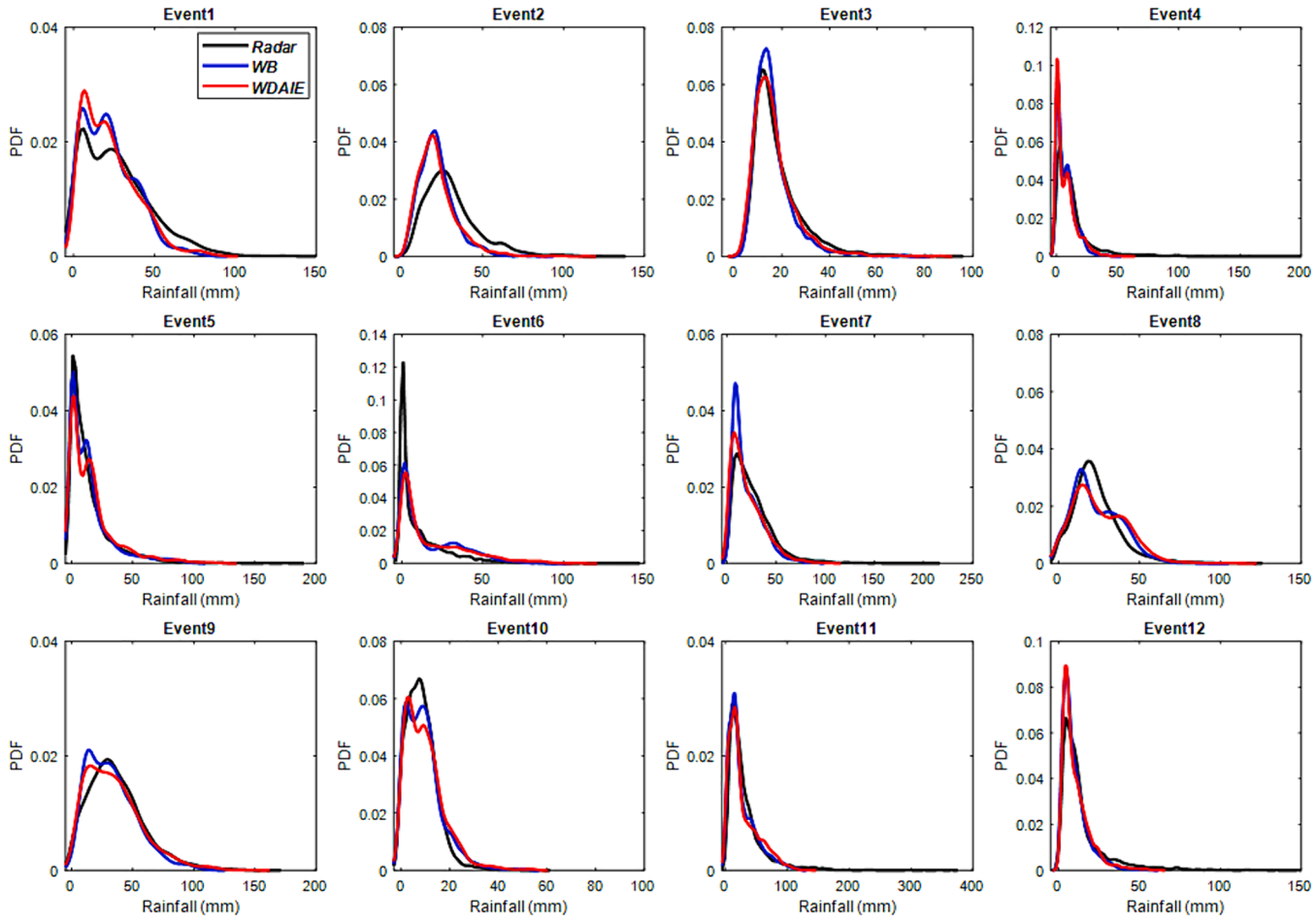

Fig. 11. Probability Density Function (PDF) of rainfall for Events 1–12. The black, blue and red lines are the results of radar, WB and WDAIE simulations respectively. (For interpretation of the references to colour in this figure legend, the reader is referred to the web version of this article.)

involving various aerosols, especially some anthropogenic aerosols (such as SO_4, NO_3, NH_4 and BC). As mentioned in Section 4.2, the atmosphere in winter and autumn has significantly higher Na and Cl aerosol mass concentrations than in spring and summer (Fig. 5), which may also be one of the reasons for the better simulation performances of the former. This can be demonstrated by different rainfall events in the same season. For example, winter Event 3 (ranked 1st; involved Na, Cl, and OIN) versus Event 1 (ranked 4th; involved Na, Cl, NO_3, OC, OIN), autumn Event 10 (ranked 2nd; involved Na and Cl) versus Event 11 (ranked 8th; involved SO_4, NO_3, OC, OIN), and summer Event 8 (ranked 6th; involved Na and Cl) versus Event 6 (ranked 12th; involved SO_4, NO_3, NH_4, BC, OC, OIN). This pattern is also consistent for most rainfall events. Especially, the summer's Event 8 got a relatively nice simulation even better than the two autumn events. In addition, it is found that the dominant aerosol components of rainfall events are strongly related to their transport sources. All components of air masses that come directly from AR or AT to the study area, or the components of air masses that influence rainfall, are mainly SSA. However, if the air mass originates from or passes through Europe (including CE, WE and NE), the air mass composition will be more complex and aerosol-induced rainfall will be subject to multiple influences. Due to this aerosol source characteristic, rainfall events influenced by long-range aerosol transport from the Arctic and Northern Atlantic Ocean have better model simulation performance than rainfall events influenced by aerosol transport from Europe under similar seasonal meteorological conditions. A notable example is comparing Event 6 affected by CE aerosols and Event 8 affected by AR aerosols. They are both autumn events but the former's performance score was approximately 55 % of the latter's. Generally, the overall performance of rainfall simulation is determined by multiple factors including aerosol properties (SSA better than anthropogenic aerosol), transport (AT/AR better than CE/WE/NE), and seasonality (winter/autumn better than spring/summer; storm better than thunderstorm/localized rainfall).

On the other hand, the greatest improvement was found for simulations that were dominated by SSA aerosols and also involved some other anthropogenic aerosols (Table 5). For example, the overall performance of events 1, 12, and 4 improved by 2.3 %, 2.2 %, and 1.0 % respectively. During these events, SSA aerosol concentration levels are higher than other events in the same season and there are obvious changes in NO_3 or SO_4. However, simulations involving only SSA aerosols showed mixed results when considering aerosol contributions, with some improving, some deteriorating and others remaining unchanged. In addition, the rainfall simulations mainly promoted by anthropogenic aerosols all experiencing performance declines in the WDAIE simulations (i.e. Events 9, 11 and 6), which indicates the model's limitations in effectively handling the effects of substantial anthropogenic aerosol. Especially for Event 6 which was entirely influenced by CE anthropogenic aerosols, it had an already low overall score of 0.48 in the WB simulation and saw a further 7.1 % decrease in the WDAIE simulation. In total, among the 12 rainfall events across in this study, turning on aerosol effects led to an improvement in simulation performance for 42 % of the events, a decrease for another 42 %, and no significant impact on the remaining 16 %. And the extent of performance improvement does not appear to have a clear correlation with rainfall intensity, season, and aerosol trajectory categories.

Finally, Event 3 as a winter storm originated from AR and was

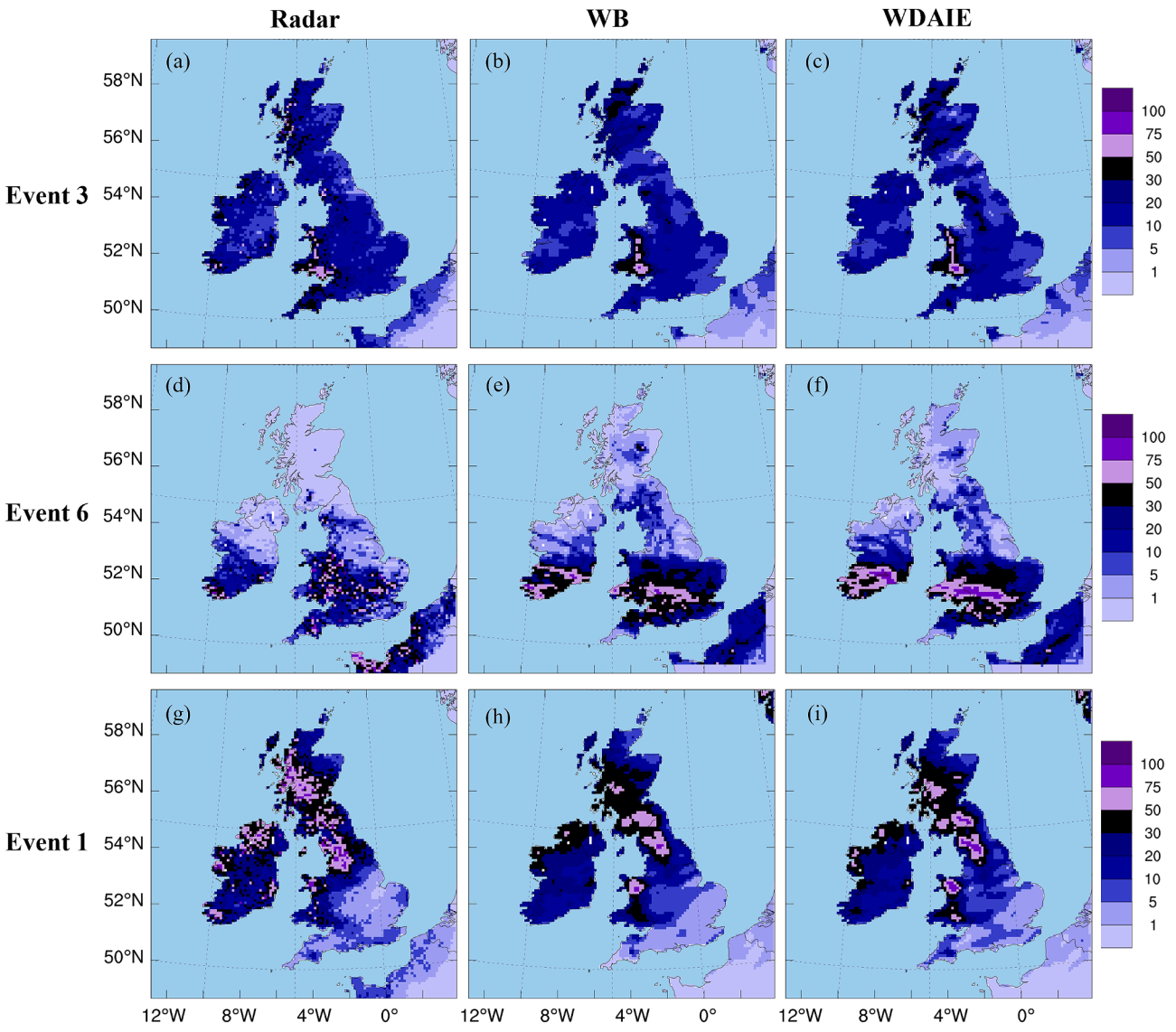

Fig. 12. Accumulated rainfall maps for the best-performing event (Event 3), the worst-performing event (Event 6) and the most-improved event (Event 1). (a, d, g) the observations of radar, (b, e, h) the results of WB simulations and (c, f, i) the results of WDAIE simulations.

promoted by Na, Cl and OIN aerosols achieved the best overall performance score of 0.891, while Event 6 as a summer thunderstorm originated from CE and was driven by SO_4, NO_3, NH_4, BC, OC, OIN aerosols scored the lowest at 0.446. Event 6 also experienced the largest decline (-7.1 %) after taking aerosol effects into account. The case with the largest improvement is Event 1, whose overall performance of the WDAIE simulation is improved by 2.3 % compared to the WB simulation. It is a winter storm that came from AR and passed through CE and WE, which is dominated by SSA aerosol and accompanied by some NO_3, OC, and OIN contributions. The accumulated rainfall maps of WDAIE simulation, WB simulation and radar observations for these three important events are highlighted in Fig. 12. It can be found that the simulated rainfall intensity and distribution of Event 3 are highly consistent with observations (Fig. 12 (a)-(c)). The shape of the PDF for Event 3 in Fig. 11 also shows a good agreement in the distribution of rainfall intensities between simulations and observations. In contrast, simulations of Event 6 had much larger accumulated rainfall in some areas than observations and this became more severe in the WDAIE simulation (Fig. 12 (d)-(f)). Its PDF reveals that the model greatly underestimated the frequency of light rainfall and overestimated the frequency of heavy rainfall. As for Event 1, the improvement from WDAIE to WB simulations is considerable in terms of spatial rainfall distributions, especially for extreme rainfall in Scotland and the North West regions (Fig. 12 (g)-(i)). The distribution of different rainfall intensities also changes significantly, making the shape of the PDF for WDAIE (red line) more similar to the observations (blue line) than WB (blue line). The accumulated rainfall maps of WDAIE simulations, WB simulations and radar observations for all 12 events can be found in Fig. S3-S6 in the Supplement.

5. Summary and conclusions

In this study, the impacts of aerosol properties (particle mass size distribution, different aerosol component variation), transport (aerosol source and trajectory) and seasonality (temperature, pressure, relative humidity, water vapor mixing ratio and wind speed) on the performances of rainfall simulations over UK and Irland for four different season months of 2020 have been evaluated through regional climate model WRF-Chem. Two sets of simulations, WB and WDAIE, were conducted to investigate the model's ability to handle aerosol effects and aerosol-cloud-precipitation-meteorology interaction under various circumstances. The model-simulated meteorological parameters were

verified using ground observations (Radiosonde and NIMROD radar dataset) and satellite measurements (AIRS) over the study area. The simulation performance of 12 extreme rainfall events during four study months was quantified through six spatiotemporal indicators *POD, FBI, CSI, FAR, RMSE* and *R*, and unified into an overall score for further analysis. Based on the 5-day backward trajectories of the HYSPLIT model, events were classified into different trajectory categories. The variations of different aerosol components (including Na, Cl, SO_4, NO_3, NH_4, BC, OC, and OIN) over time were analysed to determine the dominant aerosols for different rainfall events. Finally, the impacts of aerosol and meteorological factors on the overall performances of rainfall simulations and the performance improvements between WDAIE and WB simulations were comprehensively evaluated. The main findings and highlights of this work are as follows:

1. The model demonstrates markedly superior performance in simulating rainfall dominated by Na and Cl compared to its ability to simulate rainfall involving anthropogenic aerosols like SO_4, NO_3, NH_4, and BC. When activating the aerosol effect, the most significant performance improvements relative to baseline simulations are observed in rainfall simulations with higher concentrations of SSA and the participation of anthropogenic aerosols.
2. Under similar seasonal conditions, the model performs better in simulating rainfall caused by air masses transported from the Arctic or Northern Atlantic Ocean (AR/AT) than by air masses transported from or passing through Europe (WE/CE/NE). This discrepancy arises because the easterly winds from industrialized areas of continental Europe frequently carry high anthropogenic pollution, while westerly winds wind from the Arctic or North Atlantic Ocean usually bring a large amount of sea salt aerosols.
3. Rainfall simulations for winter and autumn events outperform those for spring and summer events. This can be attributed to the strong synoptic backgrounds in autumn and winter such as the frequent occurrence of Atlantic depressions, heavy westerly winds, high concentrations of SSA aerosols and widespread storms.
4. Among the 12 study events, turning on aerosol effects led to enhanced simulation performance for 42 % of the events, a decline in performance for another 42 %, and no noticeable impact on the final 16 %. The extreme rainfall events promoted only by anthropogenic aerosols all experience performance reductions, which indicates the model's limited capability to handle the effects of substantial anthropogenic aerosol. Furthermore, there seems to be no obvious relationship between the degree of performance improvement and factors such as rainfall intensity, season and aerosol trajectories.
5. Most of the heavy rainfalls are concentrated in Scotland, Wales, North West and South West of England due to the orographic enhancement effect. When taking aerosol direct and indirect effects into account, monthly rainfall in the UK and Ireland increased significantly and resulted in a reduction in the mass of aerosols across all particle sizes. Cl reduces most in the larger size bins (625 nm to 10 μm) while NO_3 reduces most in the small size bin (39 nm to 625 nm).

This study brings out the fact that the performances of rainfall simulations over the UK and Irland are greatly impacted by aerosol properties, transport and seasonality. Moreover, these impacts exhibit a high degree of regularity due to the geographical features of the study area. Understanding the patterns of these impacts can help identify problems in the modelling process, improve the performance of rainfall simulations over the study area and further explore aerosol-cloud-precipitation-meteorology interactions. The limitation of this study is that it only deeply investigated 12 representative extreme events that focused on the UK and Ireland. The results of this study will be helpful to other similar coastal countries and low-emission regions, while the complex aerosol impacts in various types of regions around the world still need to be further compared and summarized. In future, it is hoped that our understanding of these tiny rainfall makers become deeper, enhancing our ability to accurately predict extreme weather events and effectively develop strategies for natural disasters.

CRediT authorship contribution statement

Ying Liu: Conceptualization, Data curation, Formal analysis, Investigation, Methodology, Software, Validation, Visualization, Writing – original draft, Writing – review & editing. **Hai Liu:** Software, Visualization. **Lu Zhuo:** Conceptualization, Supervision, Writing – review & editing. **Dawei Han:** Supervision, Writing – review & editing.

Declaration of competing interest

The authors declare that they have no known competing financial interests or personal relationships that could have appeared to influence the work reported in this paper.

Data availability

Data will be made available on request.

Acknowledgement

The first author is grateful to the China Scholarship Council and the University of Bristol for providing the joint scholarship (CSC No, 201908310086) for her PhD study at the University of Bristol. All authors acknowledge the dataset developers from NASA, NCAR, ECMWF and Met Office for producing and sharing the datasets used in this study. We would also like to acknowledge the Advanced Computing Research Centre at the University of Bristol for providing access to the High-Performance Computing system BlueCrystal Phase 4.

Appendix A. Supplementary data

Supplementary data to this article can be found online at https://doi.org/10.1016/j.jhydrol.2024.131806.

References

Albrecht, B.A., 1989. Aerosols, cloud microphysics, and fractional cloudiness. Science 245 (4923), 1227–1230.

Artaxo, P., Gerab, F., Yamasoe, M.A., Martins, J.V., 1994. Fine mode aerosol composition at three long-term atmospheric monitoring sites in the Amazon Basin. Journal of Geophysical Research: Atmospheres 99 (D11), 22857–22868.

AIRS project, Aqua/AIRS L3 Monthly Standard Physical Retrieval (AIRS-only) 1 degree x 1 degree V7.0 Earth Sciences Data and Information Services Center (GES DISC), 2023 2019 Greenbelt, MD, USA, Goddard 10.5067/UBENJB9D3T2H [Accessed 7 August 2023].

Bougiatioti, A., Nenes, A., Fountoukis, C., Kalivitis, N., Pandis, S.N., Mihalopoulos, N., 2011. Size-resolved CCN distributions and activation kinetics of aged continental and marine aerosol. Atmospheric Chemistry and Physics 11 (16), 8791–8808.

Braun, R.A., Aghdam, M.A., Bañaga, P.A., Betito, G., Cambaliza, M.O., Cruz, M.T., Lorenzo, G.R., MacDonald, A.B., Simpas, J.B., Stahl, C., Sorooshian, A., 2020. Long-range aerosol transport and impacts on size-resolved aerosol composition in Metro Manila. Philippines. Atmospheric Chemistry and Physics 20 (4), 2387–2405.

Browning, K.A., Hill, F.F., Pardoe, C.W., 1974. Structure and mechanism of precipitation and the effect of orography in a wintertime warm sector. Quarterly Journal of the Royal Meteorological Society 100 (425), 309–330.

Buchanan, C.M., Beverland, I.J., Heal, M.R., 2002. The influence of weather-type and long-range transport on airborne particle concentrations in Edinburgh. UK. Atmospheric Environment 36 (34), 5343–5354.

Buchholz, R. R., Emmons, L. K., Tilmes, S., & The CESM2 Development Team, 2019. CESM2.1/CAM-chem Instantaneous Output for Boundary Conditions. UCAR/NCAR - Atmospheric Chemistry Observations and Modeling Laboratory, https://rda.ucar.edu/datasets/ds313.7/ [Accessed 7 August 2023].

Carrico, C.M., Kus, P., Rood, M.J., Quinn, P.K., Bates, T.S., 2003. Mixtures of pollution, dust, sea salt, and volcanic aerosol during ACE-Asia: Radiative properties as a function of relative humidity. Journal of Geophysical Research: Atmospheres 108 (D23).

Chen, Y., Cheng, Y., Ma, N., Wolke, R., Nordmann, S., Schüttauf, S., Ran, L., Wehner, B., Birmili, W., van der Gon, H.A., Mu, Q., 2016. Sea salt emission, transport and influence on size-segregated nitrate simulation: a case study in northwestern Europe by WRF-Chem. Atmospheric Chemistry and Physics 16 (18), 12081–12097.

Chen, J.P., Hazra, A., Shiu, C.J., Tsai, I.C. and Lee, H.H., 2008. Interaction between aerosols and clouds: current understanding. Recent Progress in Atmospheric Sciences: Applications to the Asia-Pacific Region, pp.231-281.
Chen, J.P., Lamb, D., 1994. Simulation of cloud microphysical and chemical processes using a multicomponent framework. Part I: Description of the microphysical model. Journal of Atmospheric Sciences 51 (18), 2613–2630.
Cheng, F., Zhang, J., He, J., Zha, Y., Li, Q., Li, Y., 2017. Analysis of aerosol-cloud-precipitation interactions based on MODIS data. Advances in Space Research 59 (1), 63–73.
Crippa, M., Solazzo, E., Huang, G., Guizzardi, D., Koffi, E., Muntean, M., Schieberle, C., Friedrich, R., Janssens-Maenhout, G., 2020. High resolution temporal profiles in the Emissions Database for Global Atmospheric Research. Scientific Data 7 (1), 121.
Divakarla, M.G., Barnet, C.D., Goldberg, M.D., McMillin, L.M., Maddy, E., Wolf, W., Zhou, L., Liu, X., 2006. Validation of Atmospheric Infrared Sounder temperature and water vapor retrievals with matched radiosonde measurements and forecasts. Journal of Geophysical Research: Atmospheres 111 (D9).
Douglas, C.K.M., Glasspoole, J., 1947. Meteorological conditions in heavy orographic rainfall in the British Isles. Quarterly Journal of the Royal Meteorological Society 73 (315–316), 11–42.
Dusek, U., Reischl, G.P., Hitzenberger, R., 2006. CCN activation of pure and coated carbon black particles. Environmental Science & Technology 40 (4), 1223–1230.
Emmons, L.K., Walters, S., Hess, P.G., Lamarque, J.F., Pfister, G.G., Fillmore, D., Granier, C., Guenther, A., Kinnison, D., Laepple, T.J.G.M.D., Orlando, J., 2010. Description and evaluation of the Model for Ozone and Related chemical Tracers, version 4 (MOZART-4). Geoscientific Model Development 3 (1), 43–67.
Escudero, M., Stein, A., Draxler, R.R., Querol, X., Alastuey, A., Castillo, S., Avila, A., 2006. Determination of the contribution of northern Africa dust source areas to PM10 concentrations over the central Iberian Peninsula using the Hybrid Single-Particle Lagrangian Integrated Trajectory model (HYSPLIT) model. Journal of Geophysical Research: Atmospheres 111 (D6).
Grell, G.A., Dévényi, D., 2002. A generalized approach to parameterizing convection combining ensemble and data assimilation techniques. Geophysical Research Letters 29 (14), 38.
Guenther, A., Karl, T., Harley, P., Wiedinmyer, C., Palmer, P.I., Geron, C., 2006. Estimates of global terrestrial isoprene emissions using MEGAN (Model of Emissions of Gases and Aerosols from Nature). Atmospheric Chemistry and Physics 6 (11), 3181–3210.
Harrison, D.L., Driscoll, S.J., Kitchen, M., 2000. Improving precipitation estimates from weather radar using quality control and correction techniques. Meteorological Applications 7 (2), 135–144.
He, J., Zhang, L., Yao, Z., Che, H., Gong, S., Wang, M., Zhao, M., Jing, B., 2020. Source apportionment of particulate matter based on numerical simulation during a severe pollution period in Tangshan. North China. Environmental Pollution 266, 115133.
Hersbach, H., Bell, B., Berrisford, P., Hirahara, S., Horányi, A., Muñoz-Sabater, J., Nicolas, J., Peubey, C., Radu, R., Schepers, D., Simmons, A., 2020. The ERA5 global reanalysis. Quarterly Journal of the Royal Meteorological Society 146 (730), 1999–2049.
Hung, H.M., Hsu, C.H., Lin, W.T., Chen, Y.Q., 2016. A case study of single hygroscopicity parameter and its link to the functional groups and phase transition for urban aerosols in Taipei City. Atmospheric Environment 132, 240–248.
Hwang, C.L., Yoon, K., 1981. Methods for multiple attribute decision making. Multiple Attribute Decision Making: Methods and Applications a State-of-the-Art Survey 58–191.
Iacono, M.J., Delamere, J.S., Mlawer, E.J., Shephard, M.W., Clough, S.A., Collins, W.D., 2008. Radiative forcing by long-lived greenhouse gases: Calculations with the AER radiative transfer models. Journal of Geophysical Research: Atmospheres 113 (D13).
Jacobson, M.Z., Kaufman, Y.J., Rudich, Y., 2007. Examining feedbacks of aerosols to urban climate with a model that treats 3-D clouds with aerosol inclusions. Journal of Geophysical Research: Atmospheres 112 (D24).
Jiang, Y., Yang, X.Q., Liu, X., 2015. Seasonality in anthropogenic aerosol effects on East Asian climate simulated with CAM5. Journal of Geophysical Research: Atmospheres 120 (20), 10–837.
Kaufman, Y.J., Tanré, D., Boucher, O., 2002. A satellite view of aerosols in the climate system. Nature 419 (6903), 215–223.
King, A.M., Dorling, S., 1997. PM10 particulate matter—the significance of ambient levels. Atmospheric Environment 31 (15), 2379–2381.
Kumar, K.R., Sivakumar, V., Yin, Y., Reddy, R.R., Kang, N., Diao, Y., Adesina, A.J., Yu, X., 2014. Long-term (2003–2013) climatological trends and variations in aerosol optical parameters retrieved from MODIS over three stations in South Africa. Atmospheric Environment 95, 400–408.
Levin, Z., Brenguier, J.L., 2009. Effects of pollution and biomass aerosols on clouds and precipitation: observational studies. A Scientific Review, Aerosol Pollution Impact on Precipitation, pp. 205–241.
Li, G., Wang, Y., Lee, K.H., Diao, Y., Zhang, R., 2008. Increased winter precipitation over the North Pacific from 1984–1994 to 1995–2005 inferred from the Global Precipitation Climatology Project. Geophysical Research Letters 35 (13).
Lindqvist, O., Johansson, K., Bringmark, L., Timm, B., Aastrup, M., Andersson, A., Hovsenius, G., Håkanson, L., Iverfeldt, Å., Meili, M., 1991. Mercury in the Swedish environment—recent research on causes, consequences and corrective methods. Water, Air, and Soil Pollution 55, xi–261.
Liu, Y., Chen, Y., Chen, O., Wang, J., Zhuo, L., Rico-Ramirez, M.A., Han, D., 2021. To develop a progressive multimetric configuration optimisation method for WRF simulations of extreme rainfall events over Egypt. Journal of Hydrology 598, 126237.
Liu, Y., Zhuo, L., Han, D., 2023. Developing spin-up time framework for WRF extreme precipitation simulations. Journal of Hydrology 620, 129443.
Lohmann, U., Feichter, J., 2005. Global indirect aerosol effects: a review. Atmospheric Chemistry and Physics 5 (3), 715–737.
Maki, T., Lee, K.C., Kawai, K., Onishi, K., Hong, C.S., Kurosaki, Y., Shinoda, M., Kai, K., Iwasaka, Y., Archer, S.D., Lacap-Bugler, D.C., 2019. Aeolian dispersal of bacteria associated with desert dust and anthropogenic particles over continental and oceanic surfaces. Journal of Geophysical Research: Atmospheres 124 (10), 5579–5588.
Morrison, H., Thompson, G., Tatarskii, V., 2009. Impact of cloud microphysics on the development of trailing stratiform precipitation in a simulated squall line: Comparison of one-and two-moment schemes. Monthly Weather Review 137 (3), 991–1007.
Nakanishi, M., Niino, H., 2006. An improved Mellor-Yamada level-3 model: Its numerical stability and application to a regional prediction of advection fog. Boundary-Layer Meteorology 119, 397–407.
Met Office, 2003. 1 km Resolution UK Composite Rainfall Data from the Met Office Nimrod System. NCAS British Atmospheric Data Centre, https://catalogue.ceda.ac.uk/uuid/27dd6ffba67f667a18c62de5c3456350 [Accessed 7 August 2023].
Met Office, 2007a. Met Office Albemarle High Resolution Radiosonde Data. NCAS British Atmospheric Data Centre, https://catalogue.ceda.ac.uk/uuid/f603fc6a3b2242e09822540a61a99ec6 [Accessed 7 August 2023].
Met Office, 2007b. Met Office Herstmonceux station high resolution radiosonde data. NCAS British Atmospheric Data Centre, https://catalogue.ceda.ac.uk/uuid/51b40654ef68462c818677963651a7bb [Accessed 7 August 2023].
Ramanathan, V., Carmichael, G., 2008. Global and regional climate changes due to black carbon. Nature Geoscience 1 (4), 221–227.
Randles, C.A., Russell, L.M., Ramaswamy, V., 2004. Hygroscopic and optical properties of organic sea salt aerosol and consequences for climate forcing. Geophysical Research Letters 31 (16).
Rosati, B., Christiansen, S., Dinesen, A., Roldin, P., Massling, A., Nilsson, E.D., Bilde, M., 2021. The impact of atmospheric oxidation on hygroscopicity and cloud droplet activation of inorganic sea spray aerosol. Scientific Reports 11 (1), 10008.
Rosenfeld, D., Dai, J., Yu, X., Yao, Z., Xu, X., Yang, X., Du, C., 2007. Inverse relations between amounts of air pollution and orographic precipitation. Science 315 (5817), 1396–1398.
Rosenfeld, D., Lohmann, U., Raga, G.B., O'Dowd, C.D., Kulmala, M., Fuzzi, S., Reissell, A., Andreae, M.O., 2008. Flood or drought: how do aerosols affect precipitation? Science 321 (5894), 1309–1313.
Rai, M., Kang, S., Yang, J., Chen, X., Hu, Y., Rupakheti, D., 2022. Tracing atmospheric anthropogenic black carbon and its potential radiative response over Pan-third Pole region: A synoptic-scale analysis using WRF-chem. Journal of Geophysical Research: Atmospheres 127 (6), e2021JD035772.
Schill, S.R., Collins, D.B., Lee, C., Morris, H.S., Novak, G.A., Prather, K.A., Quinn, P.K., Sultana, C.M., Tivanski, A.V., Zimmermann, K., Cappa, C.D., 2015. The impact of aerosol particle mixing state on the hygroscopicity of sea spray aerosol. ACS Central Science 1 (3), 132–141.
Schultze, M., Rockel, B., 2018. Direct and semi-direct effects of aerosol climatologies on long-term climate simulations over Europe. Climate Dynamics 50, 3331–3354.
Song, F., Leung, L.R., Lu, J., Dong, L., Zhou, W., Harrop, B., Qian, Y., 2021. Emergence of seasonal delay of tropical rainfall during 1979–2019. Nature Climate Change 11 (7), 605–612.
Stedman, J.R., 1998. The secondary particle contribution to elevated PM sub 10 concentrations in the UK. Clean Air and Environmental Protection 28.
Stein, A.F., Draxler, R.R., Rolph, G.D., Stunder, B.J., Cohen, M.D., Ngan, F., 2015. NOAA's HYSPLIT atmospheric transport and dispersion modeling system. Bulletin of the American Meteorological Society 96 (12), 2059–2077.
Stjern, C.W., Stohl, A., Kristjánsson, J.E., 2011. Have aerosols affected trends in visibility and precipitation in Europe? Journal of Geophysical Research: Atmospheres 116 (D2).
Vieno, M., Heal, M.R., Hallsworth, S., Famulari, D., Doherty, R.M., Dore, A.J., Tang, Y.S., Braban, C.F., Leaver, D., Sutton, M.A., Reis, S., 2014. The role of long-range transport and domestic emissions in determining atmospheric secondary inorganic particle concentrations across the UK. Atmospheric Chemistry and Physics 14 (16), 8435–8447.
Wang, Q., Huang, R.J., Cao, J., Tie, X., Shen, Z., Zhao, S., Han, Y., Li, G., Li, Z., Ni, H., Zhou, Y., 2016. Contribution of regional transport to the black carbon aerosol during winter haze period in Beijing. Atmospheric Environment 132, 11–18.
Wang, Y., Wang, M., Zhang, R., Ghan, S.J., Lin, Y., Hu, J., Pan, B., Levy, M., Jiang, J.H., Molina, M.J., 2014. Assessing the effects of anthropogenic aerosols on Pacific storm track using a multiscale global climate model. Proceedings of the National Academy of Sciences 111 (19), 6894–6899.
Wiedinmyer, C., Akagi, S.K., Yokelson, R.J., Emmons, L.K., Al-Saadi, J.A., Orlando, J.J., Soja, A.J., 2011. The Fire INventory from NCAR (FINN): A high resolution global model to estimate the emissions from open burning. Geoscientific Model Development 4 (3), 625–641.
Zanis, P., 2009, October.. A study on the direct effect of anthropogenic aerosols on near surface air temperature over Southeastern Europe during summer 2000 based on regional climate modeling. In: Annales Geophysicae, Vol. 27(10. Copernicus GmbH, pp. 3977–3988.
Zaveri, R.A., Easter, R.C., Fast, J.D., Peters, L.K., 2008. Model for simulating aerosol interactions and chemistry (MOSAIC). Journal of Geophysical Research: Atmospheres 113 (D13).
Zhang, R., Li, G., Fan, J., Wu, D.L., Molina, M.J., 2007. Intensification of Pacific storm track linked to Asian pollution. Proceedings of the National Academy of Sciences 104 (13), 5295–5299.
Zieger, P., Väisänen, O., Corbin, J.C., Partridge, D.G., Bastelberger, S., Mousavi-Fard, M., Rosati, B., Gysel, M., Krieger, U.K., Leck, C., Nenes, A., 2017. Revising the hygroscopicity of inorganic sea salt particles. Nature Communications 8 (1), 15883.